The Journal of Immunology

Critical Role of Zinc Transporter (ZIP8) in Myeloid Innate Immune Cell Function and the Host Response against Bacterial Pneumonia

Sannette C. Hall, Deandra R. Smith, Shetty Ravi Dyavar, Todd A. Wyatt, Derrick R. Samuelson, Kristina L. Bailey and Daren L. Knoell

J Immunol 2021; 207:1357-1370; Prepublished online 11 August 2021;
doi: 10.4049/jimmunol.2001395
http://www.jimmunol.org/content/207/5/1357

The Journal of Immunology is published twice each month by
The American Association of Immunologists, Inc.,
1451 Rockville Pike, Suite 650, Rockville, MD 20852

Print ISSN: 0022-1767 Online ISSN: 1550-6606.

Critical Role of Zinc Transporter (ZIP8) in Myeloid Innate Immune Cell Function and the Host Response against Bacterial Pneumonia

Sannette C. Hall,* Deandra R. Smith,* Shetty Ravi Dyavar,* Todd A. Wyatt,[†,‡,§] Derrick R. Samuelson,[‡] Kristina L. Bailey,[‡,§] and Daren L. Knoell*

Zinc (Zn) is required for proper immune function and host defense. Zn homeostasis is tightly regulated by Zn transporters that coordinate biological processes through Zn mobilization. Zn deficiency is associated with increased susceptibility to bacterial infections, including *Streptococcus pneumoniae*, the most commonly identified cause of community-acquired pneumonia. Myeloid cells, including macrophages and dendritic cells (DCs), are at the front line of host defense against invading bacterial pathogens in the lung and play a critical role early on in shaping the immune response. Expression of the Zn transporter ZIP8 is rapidly induced following bacterial infection and regulates myeloid cell function in a Zn-dependent manner. To what extent ZIP8 is instrumental in myeloid cell function requires further study. Using a novel, myeloid-specific, *Zip8* knockout model, we identified vital roles of ZIP8 in macrophage and DC function upon pneumococcal infection. Administration of *S. pneumoniae* into the lung resulted in increased inflammation, morbidity, and mortality in *Zip8* knockout mice compared with wild-type counterparts. This was associated with increased numbers of myeloid cells, cytokine production, and cell death. In vitro analysis of macrophage and DC function revealed deficits in phagocytosis and increased cytokine production upon bacterial stimulation that was, in part, due to increased NF-κB signaling. Strikingly, alteration of myeloid cell function resulted in an imbalance of Th17/Th2 responses, which is potentially detrimental to host defense. These results (for the first time, to our knowledge) reveal a vital ZIP8- and Zn-mediated axis that alters the lung myeloid cell landscape and the host response against pneumococcus. *The Journal of Immunology*, 2021, 207: 1357–1370.

Community-acquired pneumonia (CAP) is a leading cause of morbidity and mortality worldwide. *Streptococcus pneumoniae* (pneumococcus) is the most prevalent pathogen causing CAP in the United States,, resulting in increased hospitalizations and mortality (1–4). A major predisposing factor for the increased incidence of CAP is a decline in immune function in vulnerable populations (5). Daily dietary zinc (Zn) intake is required for human health and proper immune function. Despite this, nutritional deficiency remains prevalent within vulnerable populations (6–9). In fact, ∼17% of the world's population is at risk for inadequate zinc intake (10). Dietary Zn deficiency increases susceptibility to pathogens (11) and is associated with a higher incidence of pneumonia (12, 13), whereas Zn supplementation has been shown to reduce risk (14–16).

The mechanisms by which Zn bolsters immune function and protects against pathogen invasion remain to be fully elucidated. Zn homeostasis in mammals is tightly regulated by two major Zn transporter/carrier families known as solute carrier (SLC) family 30 and 39. The SLC39, also known as Zrt-, Irt-like proteins (ZIPs), family is composed of 14 members that primarily function to increase cytosolic Zn concentrations. Through Zn mobilization, ZIPs help regulate the function of enzymes, receptors, and transcription factors as well as cytokine and growth factor–mediated signaling pathways (17, 18). Our group was the first, to our knowledge, to reveal that the Zn transporter ZIP8 is unique relative to other family members in that it is required by myeloid-lineage cells to balance host defense and the inflammatory response against bacteria (19–21). More recently, human studies have revealed that a frequently occurring ZIP8 variant allele that leads to defective intracellular transport (rs13107325; Ala391Thr risk allele) is strongly associated with inflammation-based disorders (22, 23) and bacterial infection (24).

*Department of Pharmacy Practice and Science, College of Pharmacy, University of Nebraska Medical Center, Omaha, NE; [†]Department of Environmental, Agricultural and Occupational Health, College of Public Health, University of Nebraska Medical Center, Omaha, NE; [‡]Pulmonary Division, Department of Internal Medicine, College of Medicine, University of Nebraska Medical Center, Omaha, NE; and [§]Department of Veterans Affairs Nebraska, University of Nebraska Medical Center, Western Iowa Health Care System, Omaha, NE

ORCIDs: 0000-0002-2141-7214 (S.R.D.); 0000-0002-9273-6730 (T.A.W.); 0000-0003-2990-9042 (K.L.B.); 0000-0002-9977-2857 (D.L.K.).

Received for publication December 11, 2020. Accepted for publication June 29, 2021.

This work was supported by the Foundation for the National Institutes of Health (NIH) (HL118268 [to D.L.K.]). T.A.W. is the recipient of a U.S. Department of Veterans Affairs Research Career Scientist Award (IK6 BX003781). The University of Nebraska Medical Center Flow Cytometry Research Facility is administrated through the Office of the Vice Chancellor for Research and supported by state funds from the Nebraska Research Initiative and The Fred and Pamela Buffett Cancer Center's National Cancer Institute Cancer Support Grant. Major instrumentation has been provided by the Office of the Vice Chancellor for Research, The University of Nebraska Foundation, the Nebraska Banker's Fund, and by the NIH, National Center for Research Resources Shared Instrument Program.

Address correspondence and reprint requests to Daren L. Knoell, University of Nebraska Medical Center, NE 68198-6120. E-mail address: daren.knoell@unmc.edu

The online version of this article contains supplemental material.

Abbreviations used in this article: AM, alveolar macrophage; BAL, bronchoalveolar lavage; BMDC, bone marrow–derived DC; BMDM, bone marrow–derived macrophage; CAP, community-acquired pneumonia; DC, dendritic cell; GWAS, genome-wide association study; IPA, Ingenuity Pathway Analysis LN, lymph node; LTA, lipoteichoic acid; MFI, median fluorescent intensity; MHC-II, MHC class II; SLC, solute carrier; TPA, tris 2-pyridylmethyl amine; UNMC, University of Nebraska Medical Center; URA, upstream regulator analysis; WT, wild-type; ZIP, Zrt-, Irt-like protein; *Zip8*-KO, *Zip8* knockout; Zn, zinc; $ZnSO_4$, Zn sulfate.

In fact, the SLC39A8 (rs13107325) polymorphism is one of the most pleiotropic variants in the human genome, ranking ninth of 341 genomic regions associated with more than one human disease or trait in genome-wide association studies (GWAS) (23).

Myeloid innate immune cells, namely macrophages and dendritic cells (DCs), form the frontline defense against invading pathogens in the lungs. Both cell types express multiple pattern recognition receptors that allow for the detection of unwanted invaders and subsequent orchestration of the immune response (25). Despite the close physical proximity and functional relationships that exist between macrophages and DCs (25, 26), they are rarely examined together in the context of infectious disease.

Alveolar macrophages (AMs) are the primary resident phagocytes in the lung. They are ideal sentinels based on their location, phagocytic capacity, and expression of pattern recognition receptors. AMs employ a range of strategies to phagocytose and kill pathogens. When the capacity to clear pathogens is overwhelmed, macrophages play an important role in orchestrating the inflammatory response by secreting multiple cytokines and chemokines that recruit and activate other immune cells (25, 26). AMs have been shown to play critical roles in host defense against *S. pneumoniae*, mediating the initiation and termination of inflammation, as well as subsequent restoration of lung homeostasis (27–30).

DCs are professional APCs that bridge the gap for communication between innate and adaptive immunity. Lung DCs reside in an immature state but with the ability to quickly recognize and capture invading pathogens. Upon pathogen recognition, DCs mature, produce multiple inflammatory factors, and ultimately migrate to the draining lymph nodes, where they present processed Ags to T cells, thereby inducing Ag-specific immune responses (31, 32). A role for DCs in the pathogenesis of pneumococcal lung infection is only just emerging. Recent studies have shown that imbalance leading to excessive DC function facilitates extrapulmonary migration of *S. pneumoniae*, leading to increased inflammation, bacterial dissemination, and mortality (33, 34).

Although Zn homeostasis has an established role in mediating cellular activation against pathogens, more investigation is warranted to determine the essentiality of Zn and ZIP8 in myeloid cell function in the lung. Taken together, we hypothesized that ZIP8 plays a vital role in myeloid cell–mediated responses, especially in macrophages and DCs, and that loss of ZIP8 function will adversely impact the host response to pneumococcus through altered myeloid cell function. Using a novel myeloid-specific *Zip8* knockout (*Zip8*-KO) mouse model, we observed significant increases in cytokine production, inflammation, and mortality in *Zip8*-KO mice following pneumococcal infection. This was associated with increased lung myeloid cell infiltration and bacterial dissemination. Further in vitro analyses of macrophage and DC function revealed impaired phagocytosis and increased cytokine production upon bacterial stimulation, which was found to be, in part, due to increased NF-κB signaling. Loss of *Zip8* expression also led to profound alterations in T cell programming, which we postulate is further detrimental to host defense. These results (for the first time, to our knowledge) reveal a vital axis that involves Zn homoeostasis, myeloid cell function, and the host response against pneumococcus in the lung and reveals a molecular pathway that is accountable for the defects observed in host defense. Further study is warranted to determine whether novel micronutrient surveillance and treatment strategies can improve our ability to prevent or treat pneumococcal pneumonia.

Materials and Methods

Animals and care

All animals were maintained under specific pathogen–free conditions in the Animal Resource Facility at the University of Nebraska Medical Center (UNMC). Food and water were provided ad libitum. The research protocol used in these studies was approved by the Institutional Animal Care and Use Committee of the UNMC. All methods involving animal care and procedures in this research protocol were performed in accordance with the National Institutes of Health and Office of Laboratory Animal Welfare guidelines.

Conditional *Zip8*-KO mice were generated as previously described (35). Briefly, heterozygous $Zip8^{flox\text{-}neo/+}$ mice were bred to ROSA26:FLPe knock-in mice (The Jackson Laboratory, Bay Harbor, ME) with ubiquitous expression of FLP1 recombinase to delete the Neo cassette adjacent to the upstream loxP site. The resulting $Zip8^{flox/+}$ were mated to produce $Zip8^{flox/flox}$ mice. PCR and DNA sequencing confirmed removal of the flippase recognition target–flanked sequence and verified the loxP sites flanking exon 3. $Zip8^{flox/flox}$ mice were crossed to myeloid cell–specific LysMcre (The Jackson Laboratory) to generate the conditional *Zip8*-KO mice. LysMcre-mediated Zip8 deletion was confirmed in lung myeloid cells at baseline and 24 h after LPS stimulation using an ROSA reporter (Supplemental Fig. 1). C57BL/6J wild-type (WT) counterparts were purchased from The Jackson Laboratory and bred for experimental procedures.

Culture, quantification, and instillation of S. pneumoniae

S. pneumoniae strain JWV500 (D39hlpA-gfp-Cam'), a generous gift from Dr. J.-W. Veening (University of Lausanne), were grown to midlog phase, aliquoted, frozen, and stored at −80°C until further use. For lung infection studies, bacteria were grown to log phase in Remel Mueller Hinton Broth (Thermo Fisher Scientific, Lenexa, KS) supplemented with 32 mg/ml chloramphenicol. For quantification of pneumococci, serial dilutions of the bacteria were plated on Remel blood agar plates (Thermo Fisher Scientific) and incubated at 37°C with 5% CO_2 overnight to determine CFUs. For intranasal instillations, mice were lightly anesthetized using 2% isoflurane and 1 l/min oxygen and instilled with 4×10^8 CFUs of *S. pneumoniae* in 100 μl of PBS equally distributed (2×50 μl) between the nostrils. Mice were allowed to recover between nasal instillation doses to prevent respiratory distress. *S. pneumoniae* dose was confirmed by serial dilutions.

Bronchoalveolar lavage fluid analyses

Lungs were lavaged three times with 1 ml of ice-cold PBS. Total cell counts were determined using a hemocytometer, and differential cell counts were determined on Cytospin-prepared slides stained with Hema-3 (Thermo Fisher Scientific, Pittsburg, PA). Cytokine and chemokine levels were measured using commercially available ELISA kits according to manufacturers' instructions (BioLegend and R&D Systems).

Lung histology

Whole lungs were inflated with 10% formalin (Thermo Fisher Scientific) to preserve pulmonary architecture. Lungs were processed, paraffin embedded, sectioned (4–5 μm), and stained with H&E by the UNMC Tissue Sciences Core Facility. Slides were scanned using the VENTANA iScan HT (Roche Diagnostics, Mannheim, Germany), and images were acquired (20×) using the VENTANA Image Viewer software (Roche Diagnostics). Slides were reviewed and semiquantitatively assessed (assigned a score from 0 to 5, with a higher score indicting greater inflammatory changes) by a veterinary pathologist blinded to treatment conditions.

Tissue immunostaining

TUNEL staining. Formalin-fixed paraffin-embedded lung sections were stained for in situ apoptosis detection using the Click-IT Plus TUNEL Assay Alexa 594 (Thermo Fisher Scientific) according to manufacturer instructions. Images were visualized using a Zeiss Observer Z1 inverted phase contrast fluorescence microscope (Carl Zeiss Microscopy, White Plains, NY), and Alexa 594 fluorescent intensity was quantified using the ImageJ software (National Institutes of Health).

Caspase-3 staining. Formalin-fixed paraffin-embedded lung sections were stained for caspase-3 expression by the UNMC Tissue Sciences Core Facility using standardized protocols. Briefly, slides were stained with caspase-3 primary Ab (Abcam, Cambridge, MA), washed, incubated with anti-HRP Ab, washed, stained with H_2O_2 and DAB ChromoMap (Roche Diagnostics), and counterstained with hematoxylin. Slides were scanned using the VENTANA iScan HT (Roche Diagnostics), and images were acquired (40×) using the VENTANA Image Viewer software (Roche Diagnostics).

Tissue processing

Lung lobes were collected and perfused with digestion solution containing 1× HBSS (HyClone, GE Healthcare Life Sciences, Logan, UT), 1 mg/ml collagenase D (Roche Diagnostics), and 20 μg/ml DNase (Roche Diagnostics); incubated for 30 min at 37°C; and homogenized using gentleMACS Octo Dissociator (Miltenyi Biotec, Auburn, CA). After enzymatic digestion

and RBC lysis (1× RBC Lysis Buffer; Invitrogen by Thermo Fisher Scientific, Life Tech Corp, Carlsbad, CA), samples were resuspended in FACS rinsing buffer (1× PBS supplemented with 4% FBS and 20% sodium azide) for cell surface staining.

Isolation and generation of bone marrow–derived macrophages and DCs

Bone marrow–derived macrophages. Bone marrow–derived macrophages (BMDMs) were generated from WT and *Zip8*-KO mice (7–10 wk old) as previously described (36). Briefly, femurs and tibias were harvested from mice in both groups, and bone marrow cells were plated in DMEM containing 2 mM glutamine and supplemented with 10% FBS, penicillin/streptomycin (Life Technologies), and 20% L929 conditioned medium as a source of M-CSF. Cells were plated at a density of 5×10^5 cells/ml in 100-mm dishes. Cells were grown for 3 d, and fresh media supplemented with 20% L929 conditioned medium was added on day 3. Cells were incubated for an additional 4 d prior to further experimentation.

Bone marrow–derived DCs. Bone marrow–derived DCs (BMDCs) were generated as previously described (37), with a few modifications. Briefly, the femurs and tibias from C57BL/6 WT and *Zip8*-KO mice (7–10 wk old) were harvested, and bone marrow cells were plated in RPMI 1640 (HyClone) supplemented with 10% FBS, penicillin/streptomycin (Life Technologies), and 50 μM 2-ME (MP Biomedicals, Solon, OH) at a density of 1×10^6 cells/ml in six-well plates. The cell culture media was supplemented with 20 ng/ml recombinant mouse GM-CSF and 20 ng/ml IL-4 (PeproTech, Rocky Hill, NJ). Fresh media supplemented with GM-CSF and IL-4 (3 ml/well) was added to the plates on days 3 and 6. On day 8, the nonadherent and loosely adherent fractions were collected for CD11c isolation. Immature BMDCs (day 8) were harvested from cell culture plates, centrifuged at 250 × *g* for 10 min, resuspended in MACS buffer, and incubated with CD11c ultrapure magnetic beads (Miltenyi Biotec) according to the manufacturer's protocol. The $CD11c^+$ fraction was isolated, and cells were resuspended in DC media (RPMI 1640 supplemented with IL-4 and GM-CSF) for subsequent studies.

BMDM phagocytosis assay

Bacteria were prepared as previously described and labeled with 5 μM CFSE at 37°C for 30 min. Following CFSE labeling, bacteria were washed and incubated with WT and *Zip8*-KO BMDMs plated at a density of 5×10^5 cells/ml on 12-well plates (multiplicity of infection of 10). Plates were centrifuged at 200 × *g* for 5 min and incubated for 1 h to allow for bacteria internalization. Cells were then washed three times with ice-cold PBS to remove unbound bacteria, harvested, and stained with cell surface markers for flow cytometry. For detection of background fluorescence, BMDMs from both groups were incubated with *S. pneumoniae* at 4°C. Median fluorescent intensity (MFI) of CFSE was used as a measure of phagocytosis after subtracting the MFI of the 4°C *S. pneumoniae* sample from the 37°C *S. pneumoniae* sample (MFI $\text{CFSE}_{\text{sample}}$ = MFI $\text{CFSE}_{\text{sample @37°C}}$ − MFI $\text{CFSE}_{\text{sample @4°C}}$). To ensure viability of bacteria after CFSE labeling, aliquots were serially diluted and plated on blood agar plates to determine CFUs.

BMDC activation

BMDCs were plated at a density of 5×10^5 cells/ml on 12-well plates and incubated with either 1 μg/ml LPS from *Escherichia coli* (catalog no. L4516; MilliporeSigma, St. Louis, MO) or 10 μg/ml lipoteichoic acid (LTA) from *Staphylococcus aureus* (catalog no. L2515; MilliporeSigma) for 6 h. Cells and supernatants were harvested for downstream analyses.

FACS

BMDCs and/or whole-lung lysates were incubated with Zombie UV Fixable Viability Kit (BioLegend) at room temperature for 15 min. Cells were washed with FACS rinsing buffer, pelleted, and incubated with anti-mouse CD16/32 (BioLegend) for 15 min at 4°C to block nonspecific Ig binding. Following subsequent washing and centrifugation, cells were incubated with Ab mixtures containing some or all of the following markers: CD11c BV711, CD80 BV650, CD64 PerCP/Cy5.5, Ly-6C BV605, CCR-7 APC, MHC class II (MHC-II; I-A/I-E) BV 421, Ly-6G BV650, CD40 PE/Cy7,CD4 APC/Cy7, CD3 APC, and CD8α PerCP/Cy5.5 (BioLegend); CD86 BUV395, CD11b BV480, Siglec-F APC-R700, CD45 BV805, CD103 PE-CF594, and CD24 BUV 737 (BD Biosciences, San Jose, CA). Cells were analyzed using the BD LSRFortessa (BD Biosciences). Cell aggregates were removed by gating single cells on the forward light scatter (forward scatter height versus forward scatter area). Dead cells and debris were excluded before gating for myeloid innate immune cells and/or T cell markers. Fluorescence minus one controls were used to set up gating strategies used in these experiments. Data were analyzed using FlowJo software v10.7.1 (Tree Star).

RNA isolation and gene expression analysis

Total RNA was isolated from BMDCs using the RNeasy Mini Kit (QIAGEN, Hilden, Germany) per manufacturer's instructions and total RNA yield quantified using Nanodrop One (Thermo Fisher Scientific, Waltham, MA). The isolated RNA was then reverse transcribed using the High Capacity cDNA Transcription Kit (Applied Biosystems, Thermo Fisher Scientific). Quantitative real-time PCR was performed using the 7500 Real-Time PCR System (Applied Biosystems). Forward and reverse primers used were as follows: *Zip6* 5′- ACAACGCTGTCTCTGAAGGA-3′ and 5′-AAGCTCTTTCTGGGCTCACT-3′; *Zip8* 5′-CAGTTGCTGTGTTTGGTGGA-3′ and 5′-GCATAGCAAGTCACACCGTT-3′; *Zip10* 5′-TGTTGAAAGGACTTGTGGCG-3′ and 5′-TACCGAGTCATCCGTTCCAG-3′; and *Zip14* 5′-GGAAGATCTCATGGACCGCT-3′ and 5′-AGAATGGTGGGGCAGAACTC-3′ (Integrated DNA Technologies, Coralville, IA). Relative gene expression was normalized against the housekeeping gene GAPDH, and fold change in mRNA expression was determined using the $^{\Delta\Delta}$Ct method (38).

Gene expression profiling was performed using the NanoString nCounter system (NanoString Technologies, Seattle, WA). Specifically, mouse myeloid cell innate immune response genes were profiled using the nCounter Mouse Myeloid Innate Immunity Panel v2 according to the manufacturer's instructions. Briefly, 50 ng of total RNA per sample was hybridized overnight and loaded on to a cartridge via the nCounter MAX/FLEX System, set to the high-sensitivity setting. The cartridge was stored overnight, in the dark, at 4°C before loading onto the nCounter Digital Analyzer. Gene expression was normalized against 20 internal reference genes, and data analysis was performed using nSolver 4.0 Analysis Software (NanoString Technologies).

Ingenuity Pathway Analysis (IPA) software (Qiagen) was used to perform pathway enrichment, gene network, and upstream regulator analyses (URA) according to the standard protocols as previously described (39, 40). A list of differentially expressed genes in a dataset with a minimum of 1.5-fold change and p value of <0.05 significance were compared between the two groups and uploaded into IPA. Core analysis was performed on uploaded datasets based on fold change and p value significance to determine the biological pathways significantly (<0.05 p value and >0.05 ratio of differentially regulated genes involved in a pathway with the number of genes associated with the pathway) regulated in a dataset according to a standard protocol as previously described (41). A gene transcriptional network analysis was performed to identify transcripts that were significantly regulated, and part of a transcriptional network was destined to perform a specific biological function. This, in turn, was used to mechanistically identify key or central regulators of a transcriptional network. URA was performed to identify secretory factors, signaling mediators, and transcription factors that may not have been differentially expressed at the transcription level but are predicted to be posttranslationally altered or modified (phosphorylation, acetylation, and methylation) at the protein level with significant (p value < 0.05 and Z score $> \pm 2.0$) activation or inhibition.

Western blotting

Cell lysates were obtained using standard cell lysis buffer (Cell Signaling Technology, Danvers, MA) containing 1 mM PMSF. Proteins were separated by SDS-PAGE and transferred to nitrocellulose membranes (Thermo Fisher Scientific). The membranes were blocked with 5% BSA (Sigma-Aldrich) in TBS, followed by probing for Abs overnight. All primary Abs were purchased from Cell Signaling Technology. Protein detection and analysis was done using the Odyssey Image System (Li-Cor, Lincoln, NE).

Inhibition studies

BMDCs were primed with 10 μM Bay 11-7082 (MilliporeSigma) or vehicle control for 1 h. Cells were washed three times with media and then stimulated with 1 μg/ml LPS for designated time points. Whole-cell lysates were obtained with standard cell lysis buffer (Cell Signaling Technology) containing 1 mM PMSF. Protein concentrations were obtained using the Pierce BCA Protein Assay (Thermo Fisher Scientific).

NF-κB translocation (flow cytometry)

WT and *Zip8*-KO BMDCs were primed with the inhibitor as described above, washed, and stimulated with LPS (1 μg/ml) for 15 min. Cells were harvested, washed, fixed, and permeabilized in 150 μl of Cyto-Fast Fix/Perm buffer (BioLegend) for 20 min. Following fixation, cells were washed with 1 ml Cyto-Fast Perm Wash solution, centrifuged (250 × *g* for 10 min), and resuspended in Cyto-Fast Perm Wash solution for staining. Fixed and permeabilized cells were stained with NF-κB p65 FITC (Santa Cruz Biotechnology, Dallas, TX) for 20 min at room temperature, washed, stained with

DRAQ5 (ImmunoChemistry Technologies, Bloomington, MN), and analyzed using Amnis FlowSight Imaging Flow Cytometer (Luminex, Austin, TX).

Zn quantification

Zn was semiquantified at baseline and in stimulated (LPS or LTA, 6 h) WT and *Zip8*-KO BMDCs by incubating cells with 1 μM Zinpyr-1 (Millipore-Sigma) for 30 min. Following incubation, cells were washed three times and harvested for cell surface staining (for DC markers). ZinPyr-1 fluorescent intensity was measured by FACS, and Zn levels were quantified as MFI of ZinPyr-1.

Zn chelation and supplementation

BMDCs from WT and *Zip8*-KO mice were incubated with either 1 μM tris 2-pyridylmethyl amine (TPA) or 0.1 μM Zn sulfate ($ZnSO_4$) for 30 min in Zn-free RPMI 1640. Cells were washed twice with RPMI 1640 and stimulated with 100 ng/ml of LPS for 24 h. Supernatants were collected for cytokine expression.

$CD4^+$ T cell responses in vivo and ex vivo

WT and *Zip8*-KO mice were infected with *S. pneumoniae* as previously described, and mediastinal lymph nodes were harvested 72 h postinfection. Lymph nodes were processed into single-cell suspensions, stained with an Ab mixture consisting of CD11c, MHC-II, CD24, CD64, CD80, CD86, CD40, CD45, CD3, CD8α, and CD4 (BD Biosciences and BioLegend), and DC and T cell populations were then phenotyped by flow cytometry.

To characterize $CD4^+$ Th cell subsets, lymph node cell homogenates from WT and *Zip8*-KO–infected mice were stimulated in vitro with a cell activation mixture containing PMA (10 ng/ml; STEMCELL Technologies, Vancouver, Canada), ionomycin (250 ng/ml; STEMCELL Technologies), and brefeldin A (5 μg/ml; BioLegend) for 4 h. Cells were harvested, washed, stained for surface markers as previously described, fixed and permeabilized for 20 min with CytoFastFix/Perm (BioLegend), washed, and then stained with an Ab mixture containing IL-2 APC, IL-4 PE/Dazzle594, IFN-γ PE, and IL-17 BV421 (BioLegend). Intracellular cytokine production of the $CD4^+$ T cell subset was characterized by flow cytometry.

For cytokine detection by ELISAs, lymph nodes (LN) leukocytes were stimulated with PMA (10 ng/ml) and ionomycin (250 ng/ml) for 48 h. Supernatants were collected for measurement of IL-2, IFN-γ, IL-4, and IL-17A/F according to manufacturers' instructions.

ELISA

Cytokine levels (TNF-α, IL-2, IL-4, IL-17A/F, IL-6, IL-10, IL-12/23p40, IFN-γ, and CXCL-1) were determined using commercially available ELISA kits (BioLegend and R&D Systems, Minneapolis, MN) according to manufacturers' instructions. Assay sensitivities were IL-6 and CXCL-1 (2 pg/ml); TNF-α, IFN-γ, and IL-12/23p40 (4 pg/ml); IL-10 (16 pg/ml); IL-17A/F (2.3 pg/ml); and IL-2 and IL-4 (1 pg/ml).

Statistical analyses

Data were analyzed using GraphPad Prism version 8.00 (GraphPad Software, La Jolla, CA). Unpaired Student *t* test was used to determine differences between groups. Multiple-group comparisons were made using ANOVA with Tukey post hoc tests. Values are expressed as means ± SEM. A p value ≤ 0.05 was considered significant.

Results

Loss of Zip8 is associated with increased lung injury and mortality following S. pneumoniae *infection*

To determine the role of ZIP8 in the immune response following pneumococcal infection, WT and *Zip8*-KO mice were administered a dose of 4×10^8 CFUs *S. pneumoniae* via intranasal installation and monitored over a 7-d period. *Zip8*-KO mice were observed to have increased morbidity and mortality following pneumococcal infection in the lung (Fig. 1). By the end of the fourth day postinstillation, ∼40% of the *Zip8*-KO mice had succumbed to the infection compared with only 5% in the WT group ($p < 0.01$; Fig. 1A). Based on this observation, we next examined the immune response at 72 h postinfection. Mice were administered 4×10^8 CFUs *S. pneumoniae*, and tissues were harvested for further analysis. Histological staining of lung tissue revealed that *Zip8*-KO mice had

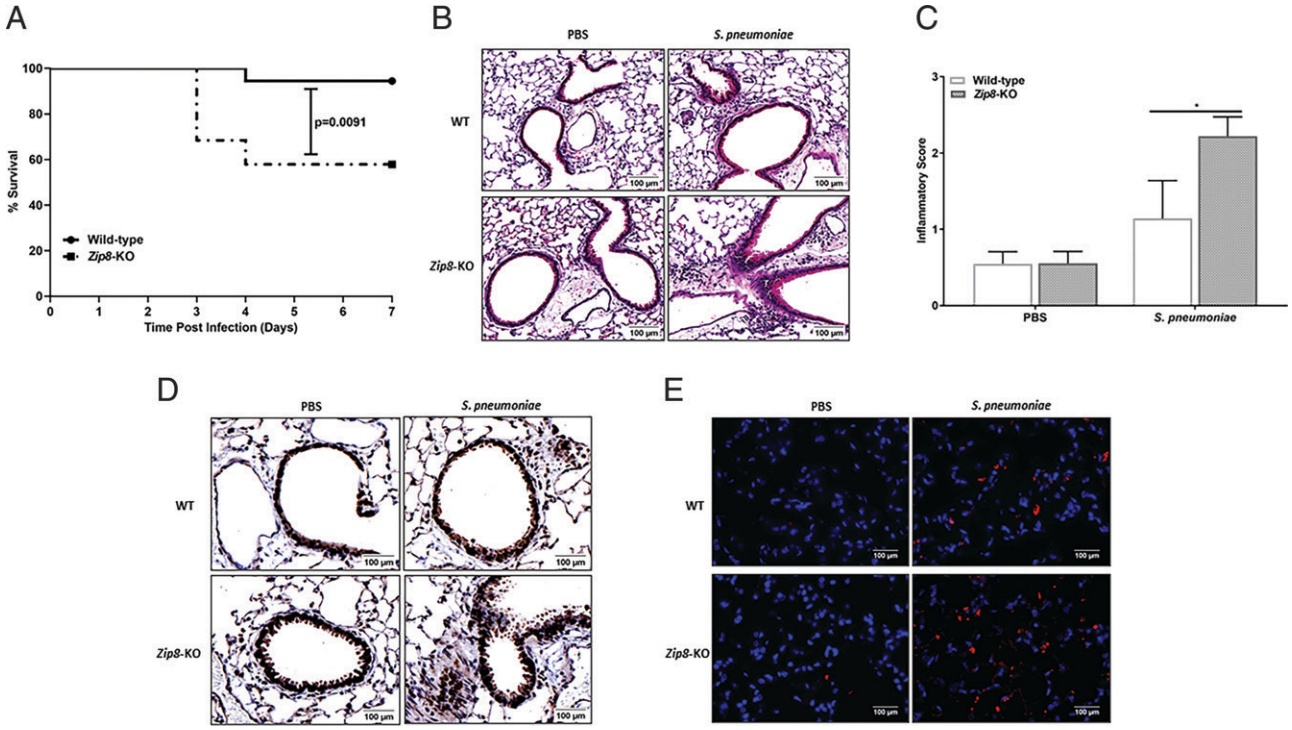

FIGURE 1. Loss of ZIP8 in myeloid cells is associated with increased mortality and lung injury following pneumococcal infection. (**A**) WT and *Zip8*-KO mice were infected with, on average, 4×10^8 CFUs of *S. pneumoniae*, and survival was monitored out to 7 d. Next, WT and *Zip8*-KO mice were infected with 4×10^8 CFUs *S. pneumoniae*, and lung samples were harvested at 72 h postinfection. Lung tissue was examined for (**B**) H&E-stained histopathology, (**C**) corresponding inflammatory scores, (**D**) caspase-3 staining, and (**E**) TUNEL staining. Caspase-3 and TUNEL staining are representative of multiple images from multiple animals. (Original magnification: ×20, H&E and ×40, caspase-3 and TUNEL staining.) Scale bars, 100 μm. Data are presented as the mean ± SEM and represent at least two independent studies. $n = 18–19$ mice per group (A), $n = 7–8$ mice per group (B)–(D). $^*p \leq 0.05$.

increased lung injury, as determined by inflammatory score, and increased cell death, as determined by TUNEL and caspase-3 staining (Fig. 1B–E). This response persisted in the surviving *Zip8*-KO mice up to 7 d postinfection as observed by histological and bronchoalveolar lavage (BAL) fluid analysis of lung tissue from survivors (Supplemental Fig. 2A–D).

Zip8-*KO increases cellular infiltration and lung inflammation within 24 h and up to 72 h following bacterial instillation*

To examine the early immune response against *S. pneumoniae* in the lung, WT and *Zip8*-KO mice were administered 4×10^8 CFUs *S. pneumoniae* and euthanized 24 or 72 h later. Analysis of BAL fluid from the lungs revealed that bacterial instillation resulted in increased total numbers of leukocytes in the airways of both groups when compared with the uninfected mice at 24 and 72 h postinfection. Macrophages and neutrophils were the main subsets of leukocytes identified. The *Zip8*-KO mice exhibited higher numbers of macrophages at 24 h postinfection, which persisted up to72 h postinfection (Fig. 2A), and higher numbers of neutrophils 24 h postinfection (Fig. 2B). Pneumococcal infection was also associated with increased expression of IL-6, TNF-α, and IL-12/23 (p40 subunit) in both groups, with IL-12/23p40 trending higher in the *Zip8*-KO group when compared with WT animals ($p = 0.055$; Fig. 2C–E). Taken together, these results demonstrate an imbalance in the cellular landscape and immune response to *S. pneumoniae* as a consequence of ZIP8 loss.

Zip8 *loss alters lung cellularity in a manner that promotes tissue injury and mortality*

Knowing that macrophages and DCs play critical roles in orchestrating the immune response after bacterial infection and that we observed increased mortality between 72 and 96 h postinfection, we next characterized the lung tissue population of both cell types, including DC subsets, at 72 h postinfection. Mice were infected with *S. pneumoniae* (4×10^8 CFUs), and tissues were harvested for further analyses. Immune cells in lung homogenates from both groups were characterized using flow cytometry. After gating out debris and doublets, live $CD45^+$ leukocytes were selected. Cells were characterized as AMs, based on expression of CD11c, Siglec-F, and CD64 ($CD45^+$ $CD11c^+$Siglec-F^+ $CD64^+$), or DCs, based on expression of classic DC markers ($CD45^+CD24^+CD64^-CD11c^+$MHC-$II^+$; Supplemental Fig. 1). DC subsets were then identified based on the expression of CD11b or CD103. There was an increase in total macrophage and DC numbers in both groups from 24 to 72 h postinfection. At 72 h postinfection, the *Zip8*-KO group exhibited increased DC numbers compared with WT animals (Fig. 3A, 3B). Further analysis of DC subsets revealed an increase in the total numbers of $CD11b^+$ DCs in the lungs of *Zip8*-KO mice (Fig. 3C), which consisted of a mix of resident/conventional DCs ($CD11b^+$Ly-$6c^-$) and overall greater numbers of inflammatory monocyte-derived DCs ($CD11b^+$Ly-$6c^+$) when compared with the WT counterparts (data not shown). These results further demonstrate that Zip8 loss aggravates the inflammatory response at least in part through alteration of the lung macrophage and DC landscape in response to pneumococcal infection.

Loss of Zip8 is associated with impaired macrophage phagocytosis and increased bacterial dissemination

To determine whether increased lung APC presence and increased lung tissue damage altered bacterial dissemination, bacterial counts were enumerated from the spleens of both groups. *Zip8*-KO mice had significantly higher bacterial burden in spleens 72 h postinfection (Fig. 4A). Given that increased numbers of macrophages were associated with increased bacterial dissemination in *Zip8*-KO mice, we questioned whether macrophage phagocytosis was impaired by ZIP8 loss. To further examine the impact of ZIP8 loss on phagocytosis, BMDMs were generated from WT and *Zip8*-KO mice and incubated with CFSE-labeled *S. pneumoniae* for 1 h, and bacterial uptake was determined by flow cytometry. Cells were gated based on expression of cell surface markers ($CD11b^+CD24^-CD64^+$), with >90% of the population phenotyped as macrophages (data not shown). Further analysis of the gated cells revealed that BMDMs generated from *Zip8*-KO mice had impaired bacterial uptake as

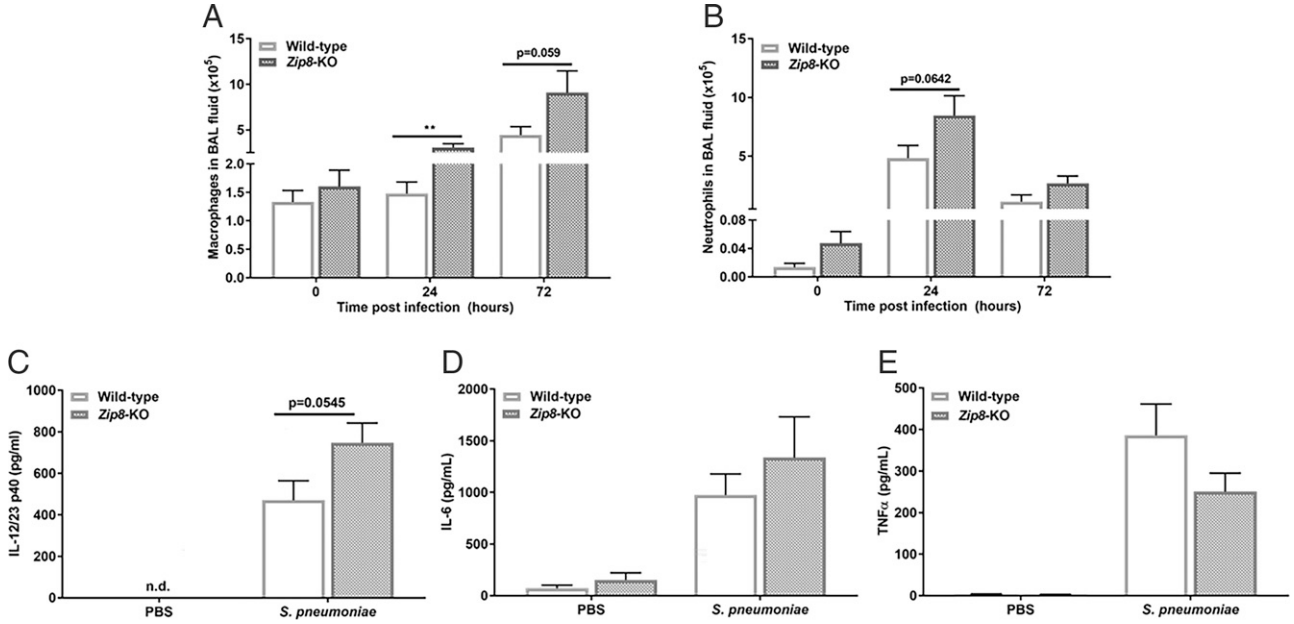

FIGURE 2. Analysis of BAL fluid for cellularity, cytokine, and chemokine content following *S. pneumoniae* instillation. WT and *Zip8*-KO mice were administered 4×10^8 CFUs *S. pneumoniae* intranasally and euthanized 24 or 72 h later. Lungs were lavaged with PBS and cells collected, counted, immobilized on glass slides, and stained for morphological characterization for (**A**) total macrophage and (**B**) neutrophil cell counts. (**C–E**) Cell-free BAL fluid was also analyzed by ELISA (C) IL-12/23p40, (D) IL-6 ,and (E) TNF-α 24 h postinfection. Data are presented as the mean ± SEM and represent at least two to three independent studies. $n = 18–19$ mice per group (24 h) and 7–8 mice per group (72 h). $^{**}p < 0.01$.

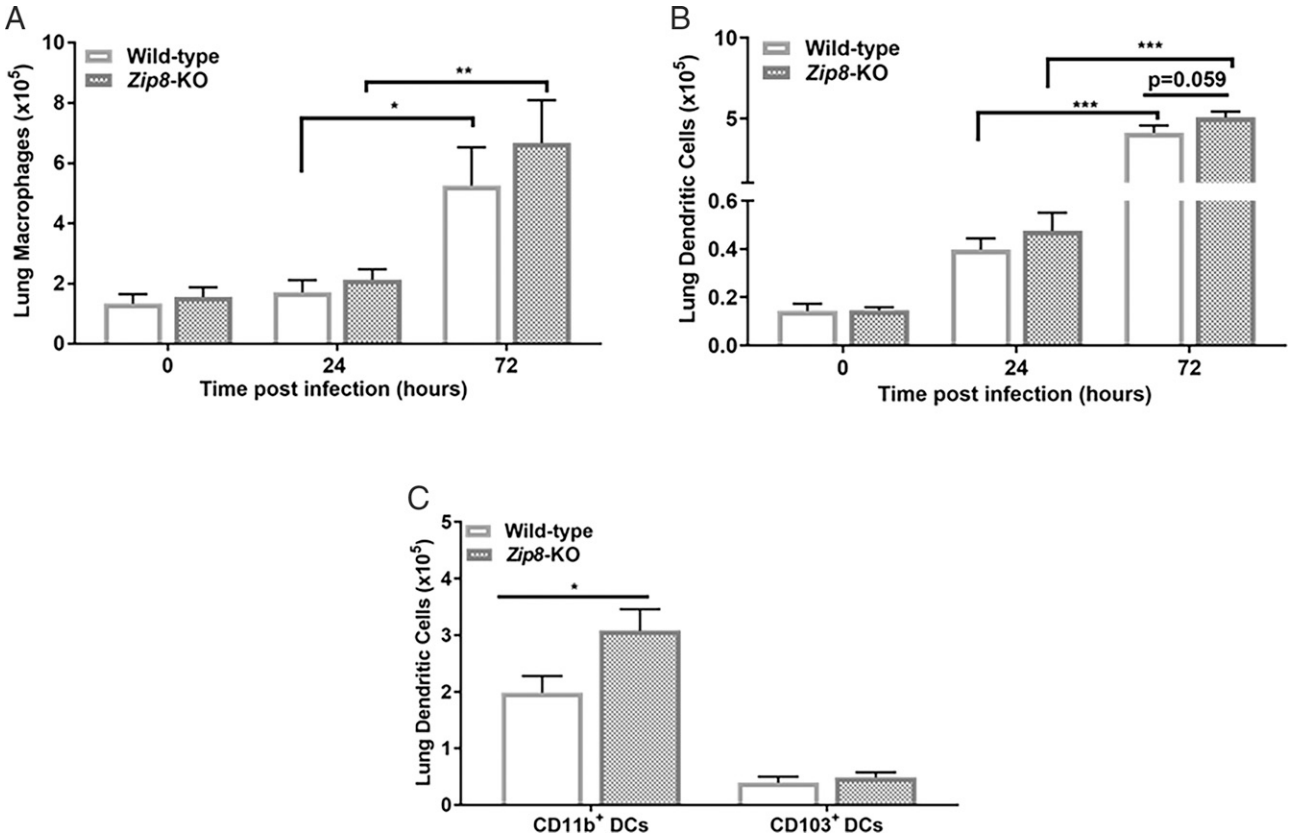

FIGURE 3. Phenotypic characterization of AMs and lung DCs 24 and 72 h after pneumococcal infection. Lung homogenates from uninfected and infected WT and *Zip8*-KO mice were phenotyped by flow cytometry analysis. After gating out debris and doublets, live $CD45^+$ leukocytes were selected. Cells were characterized as AMs, based on expression of CD11c, Siglec-F, and CD64 ($CD45^+CD11c^+Siglec\text{-}F^+CD64^+$), or DCs, based on expression of classic DC markers ($CD45^+CD24^+CD64^-CD11c^+MHC\text{-}II^+$). DC subsets were then identified based on expression of CD11b or CD103. (**A**) Quantification of total numbers of macrophages, (**B**) lung DCs, and (**C**) DC subsets in lung homogenates of *S. pneumoniae*–infected WT and *Zip8*-KO animals. Data are presented as the mean ± SEM and represent two to three independent studies. $n = 8–15$ mice per group. $^*p < 0.05$, $^{**}p < 0.01$, $^{***}p < 0.001$.

measured by the MFI of CFSE after subtracting the MFI of the control sample (4°C) from that of the test sample (37°C; Fig. 4B, 4C). Similar results were observed with *E. coli* (pHrodo Red, succinimidyl ester, *E. coli*; Thermo Fisher Scientific) up to 2 h postincubation (data not shown). These results demonstrate that ZIP8 loss significantly alters the phagocytic capacity of macrophages, which may contribute to increased bacterial dissemination as observed in *Zip8*-KO animals after pneumococcal infection.

Phenotypic characterization and cytokine production of BMDCs after bacterial stimulation

Given the increase in DCs and inflammatory cytokines observed in the lungs of *Zip8*-KO mice from 24 to 72 h postinfection, the next step was to determine whether ZIP8, or lack thereof, has direct impact on DC function as well. To examine the impact of ZIP8 loss upon DC function, BMDCs were generated from WT and *Zip8*-KO mice and then stimulated with Gram-negative and Gram-positive bacterial cell wall extracts. LPS and LTA stimulation induced a similar pattern of BMDC maturation in both groups compared with unstimulated cells. In particular, DC maturation was associated with increased expression of MHC-II, CD80/86, CD40, and CCR-7 in LPS- and LTA-pulsed WT and *Zip8*-KO BMDCs (data not shown).

Although there were no significant differences observed in maturation markers expressed by stimulated DCs from both groups, there were stark differences in the cytokine response to LPS and LTA stimulation (Fig. 5A–D). *Zip8*-KO–stimulated BMDCs had significantly higher production of IL-12/23 p40 (LPS, $p < 0.01$; LTA, $p < 0.05$), IL-6 (LPS and LTA, $p < 0.01$), and TNF-α (LTA only, $p < 0.001$). In contrast, WT BMDCs produced more IL-10 (LPS, $p < 0.001$; LTA, $p < 0.05$) compared with *Zip8*-KO cultures following stimulation. There were no differences observed in the production of CXCL-1 between the groups (Fig. 5E). Collectively, the data demonstrate that ZIP8 loss does not alter DC maturation in response to bacterial stimulation but does significantly impact internal circuitry that influences the DC immune response to both Gram-negative and Gram-positive cell wall components.

Impact of ZIP8 on bacterial stimulation and Zn homeostasis in DCs

To examine the impact of ZIP8 and Zn homeostasis on DC function in vitro, Zn transporter expression and Zn content was measured in stimulated BMDCs. Bacterial stimulation induced *Zip8* mRNA expression in WT BMDCs, which was significantly higher than in baseline and *Zip8*-KO–stimulated counterparts (LPS, $p < 0.001$; LTA, $p < 0.05$; Fig. 6A). Despite induction of *Zip8* expression, intracellular Zn content decreased in both groups following LPS and LTA stimulation. *Zip8*-KO DCs had significantly lower available Zn ($p < 0.05$) as measured by the MFI with ZinPyr-1 staining (Fig. 6B).

The observed decrease in available Zn, despite the increase in *Zip8* mRNA in the WT BMDCs, suggested that expression of other Zn transporters may be altered in stimulated BMDCs. Indeed, investigation of other select Zn transporters, namely ZIP-6, -10, and -14, revealed further changes in expression patterns, with a modest decrease in the expression of *Zip6* and *Zip10* and an increase in expression of *Zip14* relative to *Zip8* (Fig. 6C). Collectively, these observations indicate that alteration of intracellular Zn content is

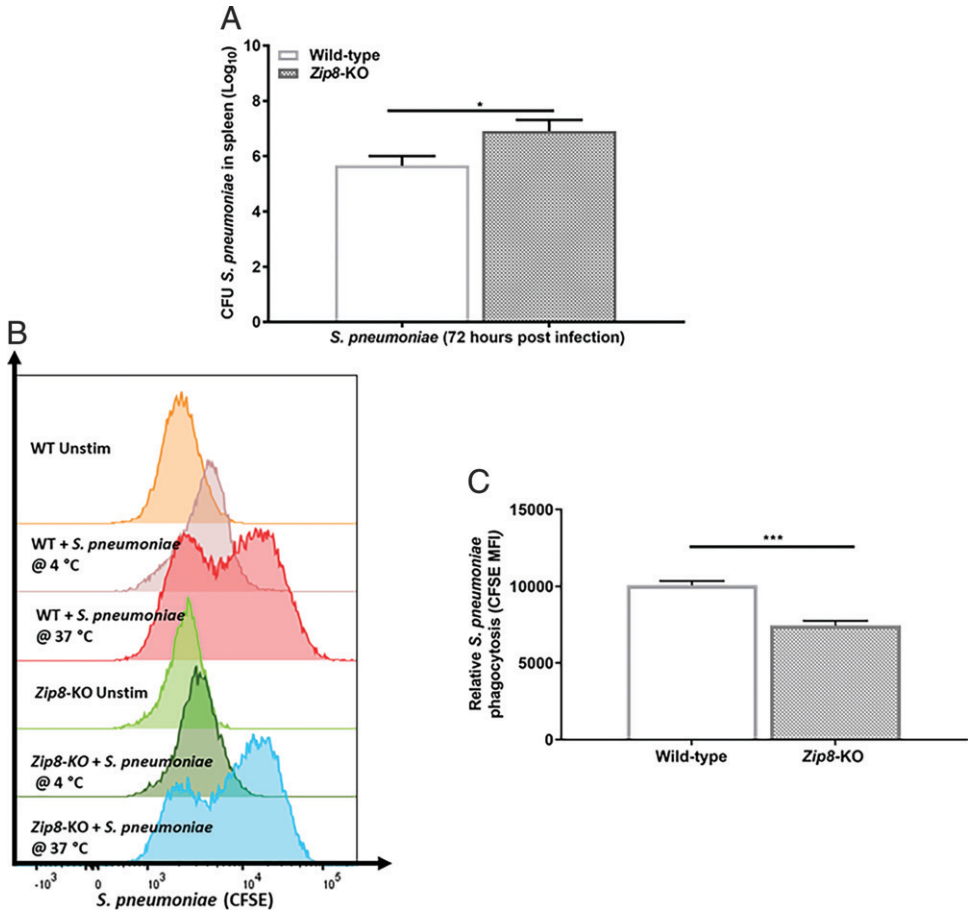

FIGURE 4. Loss of ZIP8 is associated with increased bacterial dissemination and impaired macrophage phagocytosis. (**A**) WT and *Zip8*-KO animals were infected with *S. pneumoniae* (4×10^8 CFUs), and bacterial load in spleen homogenates was assessed 72 h postinfection. BMDMs were then generated from uninfected WT and *Zip8*-KO mice and incubated with CFSE-labeled *S. pneumoniae* for 1 h, and bacterial uptake was determined by flow cytometry. Cells were gated as macrophages based on expression of cell surface markers ($CD11b^+CD24^-CD64^+$), and bacterial uptake was quantified based on CFSE expression. (**B**) Representative flow histograms of noninfected and infected cultures at 4 and 37°C. (**C**) Quantification of bacterial uptake as a measure of the MFI of CFSE, after subtracting the MFI of the control sample at 4°C from that of the test sample at 37°C (MFI $CFSE_{sample}$ = MFI $CFSE_{sample\ @37°C}$ − MFI $CFSE_{sample\ @4°C}$). Data are presented as the mean ± SEM and represent at least two independent studies. n = 10–13 mice per group (in vivo); n = 6–8 samples per group (in vitro). $^*p < 0.05$, $^{***}p < 0.001$.

consequent to altered expression of multiple Zn transporters, not excluding ZnTs, and that DCs are programmed to reduce Zn content in response to bacteria.

To further elucidate the impact of Zn homeostasis on DC responses after bacterial stimulation, BMDCs were incubated with TPA, a Zn-specific chelator, or supplemented with $ZnSO_4$ and then stimulated overnight with LPS. BMDCs treated with TPA had a net decrease in available Zn content, which was further potentiated by LPS stimulation. Comparison of baseline and treated samples revealed that WT BMDCs had significantly lower Zn content after TPA incubation and LPS stimulation (p = 0.01), whereas *Zip8*-KO BMDCs exhibited a marginal reduction in available Zn. Conversely, BMDCs treated with $ZnSO_4$ showed a marginal increase in Zn content, which was decreased after LPS stimulation in both groups (Fig. 6D).

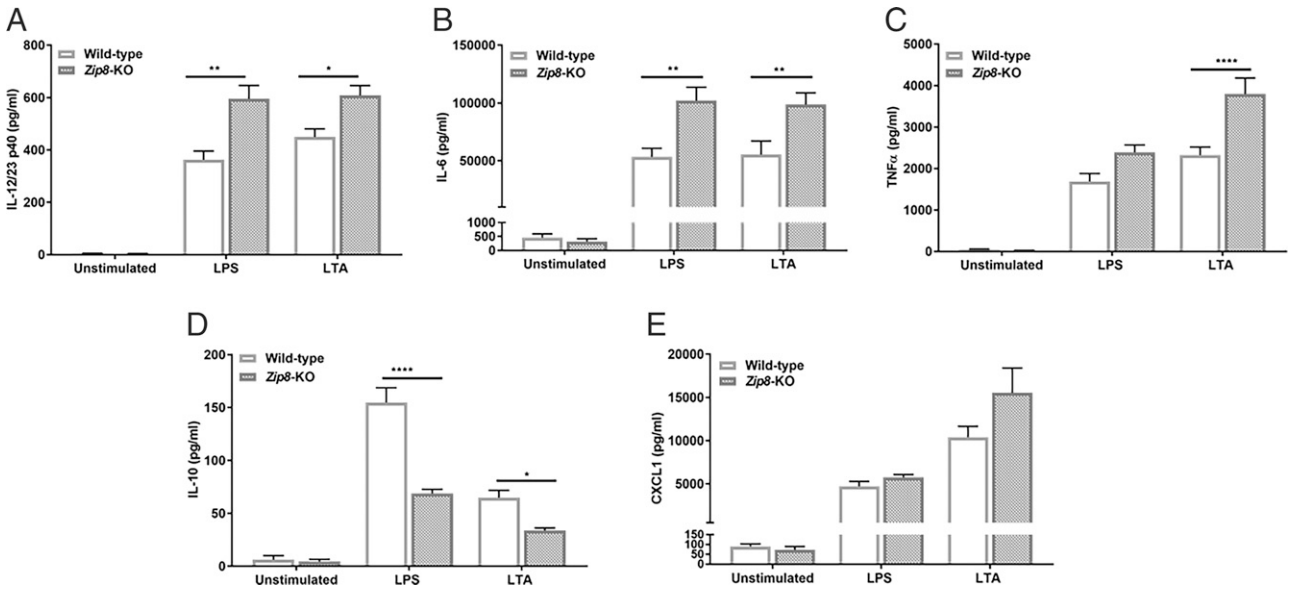

FIGURE 5. Cytokine production from BMDCs following stimulation with Gram-negative and Gram-positive bacterial cell wall products in vitro. BMDCs from WT and *Zip8*-KO mice were stimulated with either LPS (1 μg/ml) or LTA (10 μg/ml) for 6 h. (**A**–**E**) Cytokine production of IL-12/23p40, IL-6, TNF-α, IL-10, and CXCL-1 from LPS/LTA-stimulated or unstimulated BMDCs was compared and measured by ELISA. Data are presented as the mean ± SEM and represent at least four independent studies. n = 16 samples per group. $^*p < 0.05$, $^{**}p < 0.01$, $^{****}p < 0.0001$.

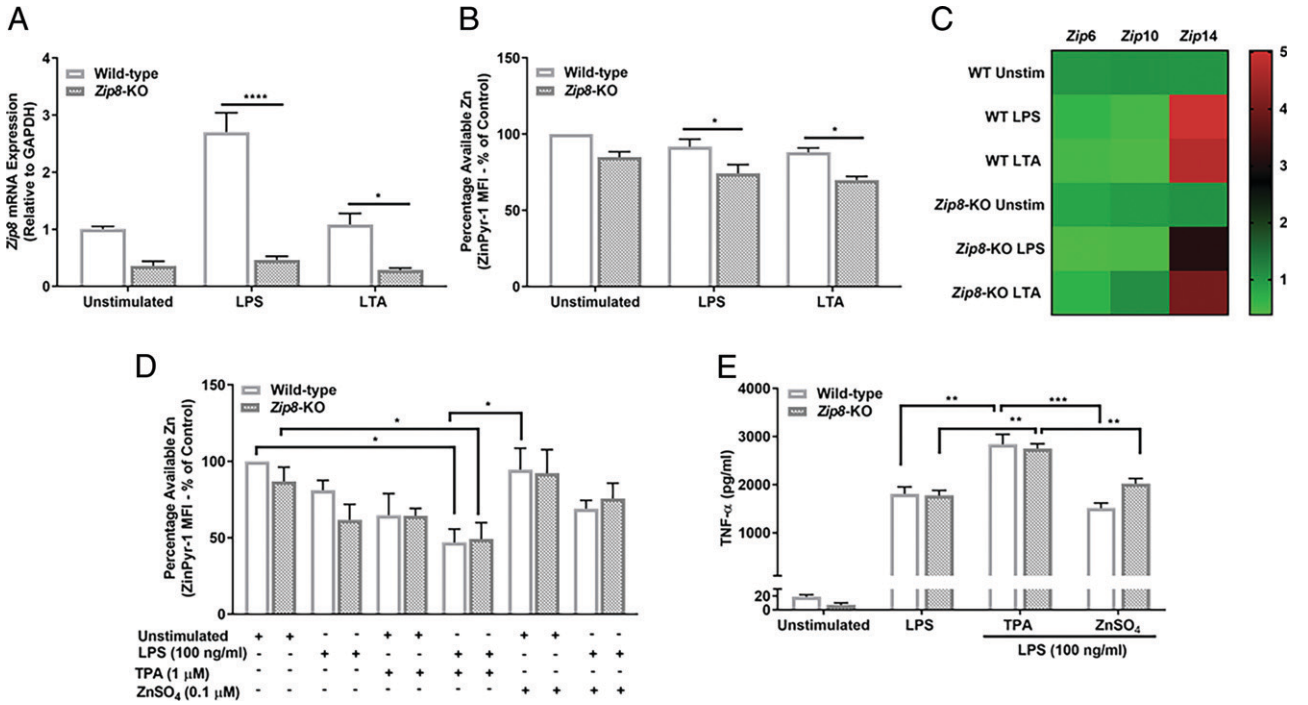

FIGURE 6. Effects of bacterial stimulation on Zn homeostasis in BMDCs. WT and *Zip8*-KO BMDCs were stimulated with LPS (1 μg/ml) or LTA (10 μg/ml) for 6 h, and cells were then harvested for analysis of select Zn transporter gene expression and cytosolic Zn content. (**A**) *Zip8* mRNA expression in WT and *Zip8*-KO BMDCs after stimulation with LPS or LTA. (**B**) Semiquantitative cytosolic Zn levels at baseline and in stimulated BMDCs as measured by ZinPyr-1 staining and FACS. Zn levels were quantified as MFI. (**C**) Heat map of gene expression of *Zip6*, *Zip10*, and *Zip14* in LPS- and LTA-pulsed BMDCs from both groups. (**D** and **E**) BMDCs from WT and *Zip8*-KO mice were then incubated with either 1 μM TPA or 0.1 μM $ZnSO_4$ for 30 min then stimulated with LPS (100 ng/ml) for 24 h. Semiquantitative cytosolic Zn expression (D) and TNF-α production (E) following Zn manipulation and LPS stimulation in BMDCs isolated from both groups. Data are presented as the mean ± SEM and represent at least three independent studies. $n = 9$ samples per group. $^*p < 0.05$, $^{**}p < 0.01$, $^{***}p < 0.001$, $^{****}p < 0.0001$.

Alteration of intracellular Zn content corresponded with changes in BMDC cytokine profiles within both groups. Reduction in intracellular Zn following chelation with TPA resulted in increased production of TNF-α in both groups ($p < 0.001$; Fig. 6E) and IL-10 but only in WT cells ($p = 0.001$; data not shown). There were, however, no differences observed in the production of IL-6 and IL-12/23p40 following Zn chelation and LPS stimulation (data not shown). Supplementation with $ZnSO_4$ had little to no effect on cytokine production between the groups, except for TNF-α production, which was significantly decreased in both groups when compared with the TPA- and LPS-stimulated samples (Fig. 6E). Collectively, these results suggest that Zn homeostasis (specifically, decreased Zn levels) contributes to differences observed in the immune response of *Zip8*-KO BMDCs following bacterial exposure.

Zip8 loss alters gene expression in DCs after bacterial stimulation

The absence of phenotypic differences between WT and *Zip8*-KO BMDCs, despite the differences seen in early cytokine production after bacterial stimulation, suggested that there may be alteration in intracellular programs that are associated with immune activation. Analysis of over 700 genes using nCounter myeloid innate immune gene profiling showed that at baseline, there were only 14 genes that were significantly different between the WT and *Zip8*-KO cells (Fig. 7A). Further comparison of baseline with bacterial-stimulated samples identified 158 genes (WT unstimulated versus bacterial stimulated) and 243 genes (*Zip8*-KO unstimulated versus bacterial stimulated) that were significantly different between the groups (Fig. 7A). Comparison of fold change in gene expression between WT and *Zip8*-KO LPS-stimulated BMDCs revealed 16 genes that were differentially expressed ($p < 0.05$), with seven of these genes highly relevant to DC function, namely, Ag presentation, chemokine/cytokine signaling, and lymphocyte activation (Fig. 7B). Using IPA, the DC maturation pathway was identified as one of the top regulatory biological pathways, involving six upregulated genes (predominantly involved in the assembly of the MHC-II molecule) from the list of differentially expressed genes in *Zip8*-KO–stimulated samples (Fig. 7B, 7C).

Given that tightly regulated gene networks are dedicated to performing specific functions in cellular transcriptomes, URA was performed to identify transcription factors and key genes controlling gene networks between treatment groups. URA predicted that the *NF-κB*, *PI3K*, and *ESR2* transcription factors were significantly upregulated in stimulated *Zip8*-KO BMDCs ($p < 0.01$ and Z score > 2.0) and may play a central role in controlling expression of gene networks (Fig. 7D). Further network analysis found that FGF2 and IFNB1 (cytokines); CCL26 and CCL6 (chemokines); and GLYRP1, HLA-DMB, CD74, and IL-10RA were integral to the NF-κB gene network in stimulated *Zip8*-KO BMDCs compared with WT BMDCs (Fig. 7E). These results show that upregulation of DC maturation pathways and activation of NF-κB–mediated signaling, through transcription factors controlling specific sets for chemokines/cytokines, could account for differences observed between LPS-stimulated BMDCs from both groups and more so in *Zip8*-KO cultures.

Increased activation of NF-κB signaling pathway in Zip8*-KO BMDCs after LPS stimulation*

To determine whether the NF-κB signaling pathway, as predicted by IPA analysis, accounted for the differences observed in DC-mediated responses between the groups, we first examined NF-κB–related molecules by phospho–Western blotting. LPS, as predicted, increased phosphorylation of IKβα in both groups, but more

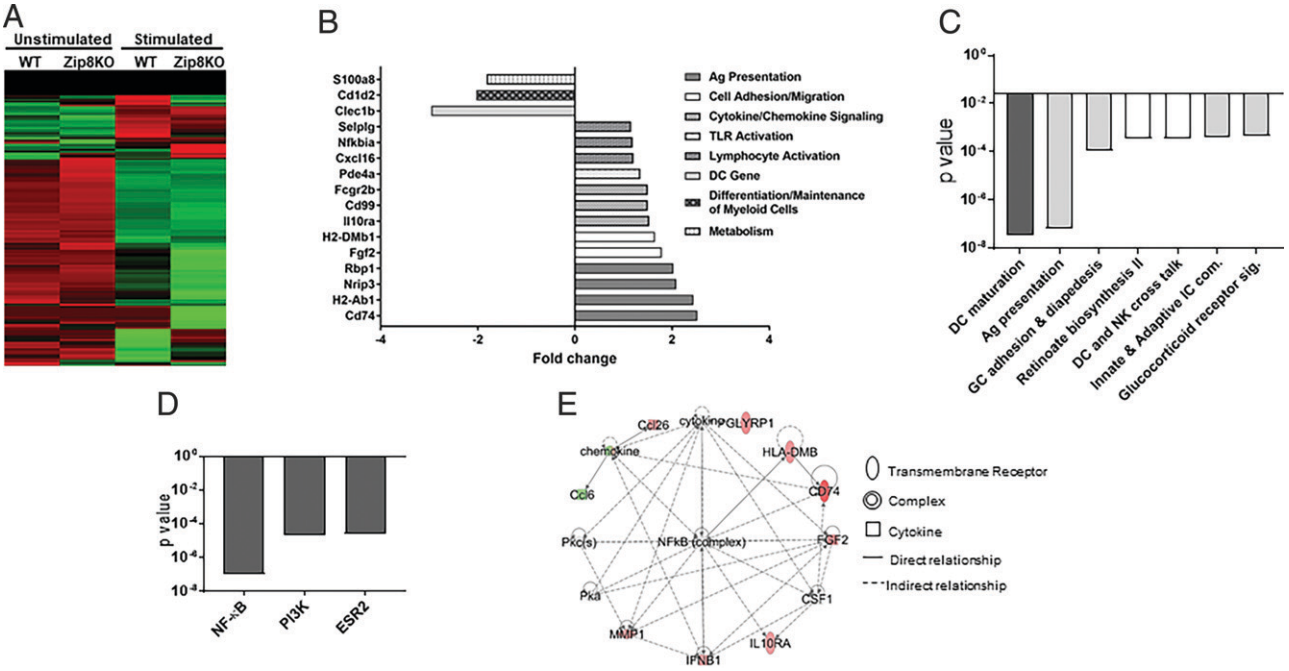

FIGURE 7. Loss of Zip8 alters the immune gene expression profile in DCs after bacterial stimulation. BMDCs were stimulated with LPS, harvested, and then RNA was isolated for NanoString and IPA analyses. (**A**) Heat map of gene expression between the WT and *Zip8*-KO unstimulated versus stimulated BMDCs. Data were generated using unsupervised clustering and normalized to a scale that gives equal variance to all the differentially expressed genes. Green indicates high and red indicates low expression. (**B**) Specific pathways significantly ($p < 0.01$) regulated in LPS-stimulated *Zip8*-KO BMDCs in comparison with WT BMDCs. Dark gray bars indicate a positive Z score; light gray bars indicate no activity pattern; and empty bars had a 0 Z score. (**C**) Fold change of genes (and associated pathways) in stimulated DCs from both groups (positive values indicate the genes that were upregulated in the *Zip8*-KO cultures) compared with WT cultures. (**D**) Upregulation of transcription factors in stimulated *Zip8*-KO BMDCs ($p < 0.0001$ and Z score > 2.0). Dark gray bars indicate a positive Z score. (**E**) NF-κB transcriptional network was identified as a leading pathway in stimulated BMDCs from *Zip8*-KO BMDCs compared with WT BMDCs. Genes that are positively (red) or negatively (green) regulated either directly or indirectly under the influence of NF-κB in *Zip8*-KO BMDCs are shown. (Data were generated from three samples per group from three independent studies.)

so in *Zip8*-KO BMDCs at 10, 15, and 30 min after stimulation. This response was attenuated in both groups after incubation with BAY 11-7082, an IKK inhibitor (Supplemental Fig. 3A). Similar results were observed with nuclear translocation of NF-κB 15 min after LPS stimulation. *Zip8*-KO BMDCs also exhibited significantly higher NF-κB translocation when compared with the WT BMDCs after LPS stimulation, which was diminished in both groups following incubation with BAY 11-7082 (Fig. 8A). Similarly, inhibition of NF-κB signaling resulted in a significant decrease in the production of IL-12/23p40, IL-6, and TNF-α in both groups following LPS stimulation (Fig. 8B–E). As observed previously, cytokine production was more pronounced in *Zip8*-KO BMDCs. The blunted cytokine response in both groups persisted up to 24 h after the stimulus was removed (Supplemental Fig. 3C–E). Interestingly, there were no differences observed in the extent of phosphorylation of other signaling molecules associated with production of these cytokines, including ERK1/2 and p38 (Supplemental Fig. 3B). These results demonstrate that the altered DC response consequent to ZIP8 loss and changes in Zn homeostasis is heavily influenced through augmentation of NF-κB signaling.

Loss of ZIP8 alters the Th2/Th17 balance after pneumococcal infection

Preliminary data from NanoString and IPA analyses predicted that ZIP8 loss is associated with changes in the expression of genes associated with Ag presentation and T cell activation. Given that DCs play a pivotal role in bridging the gap between innate and adaptive immunity and that NF-κB signaling plays a role in T cell activation by DCs (42), DCs and T cells from the mediastinal lymph nodes of WT and *Zip8*-KO mice were examined following *S. pneumoniae* infection. As previously described, mice were infected with 4×10^8 CFUs of *S. pneumoniae*, and tissues were harvested 72 h postinfection. After gating out doublets, debris, and dead cells, DCs were characterized based on expression of CD11c, MHC-II, and CD24 and further divided into two subsets based on expression of CD8α ($CD8\alpha^+$ DCs and $CD8\alpha^-$ DCs). T cells were characterized as either $CD4^+$ T cells ($CD45^+CD3^+CD4^+$) or $CD8^+$ T cells ($CD45^+CD3^+CD8^+$; Fig. 9A). Flow cytometric analysis of LN cells revealed no differences in total numbers of DC subsets ($CD8\alpha^+$ and $CD8\alpha^-$) or $CD4^+$ T cells between the groups 72 h postinfection (Fig. 9B). However, when whole LN cultures (a mix of DCs and T cells) isolated from infected animals of both groups were restimulated in vitro, stark changes in Th cell cytokine profiles were observed. Analysis of the $CD4^+$ T cell population by flow cytometry revealed a significant decrease in the production of IL-17 from the *Zip8*-KO cultures. Interestingly, this was associated with an increase in the production of IL-4, with no differences observed in the production of IFN-γ and IL-2 between the groups (Fig. 9C). Similar results were observed in *Zip8*-KO cocultures stimulated for 48 h (Fig. 9D). Collectively, results demonstrate that ZIP8 loss distorts Th2/Th17 balance in a manner that is detrimental to the host.

Discussion

In this study, we investigated the role of ZIP8 in the myeloid-mediated immune response to pneumococcal pneumonia. Strikingly, we observed that ZIP8 loss was associated with overall worse outcomes in infected mice, resulting in intensification of the inflammatory response, more collateral tissue damage and cell death, and increased mortality. Alteration of the immune response began early

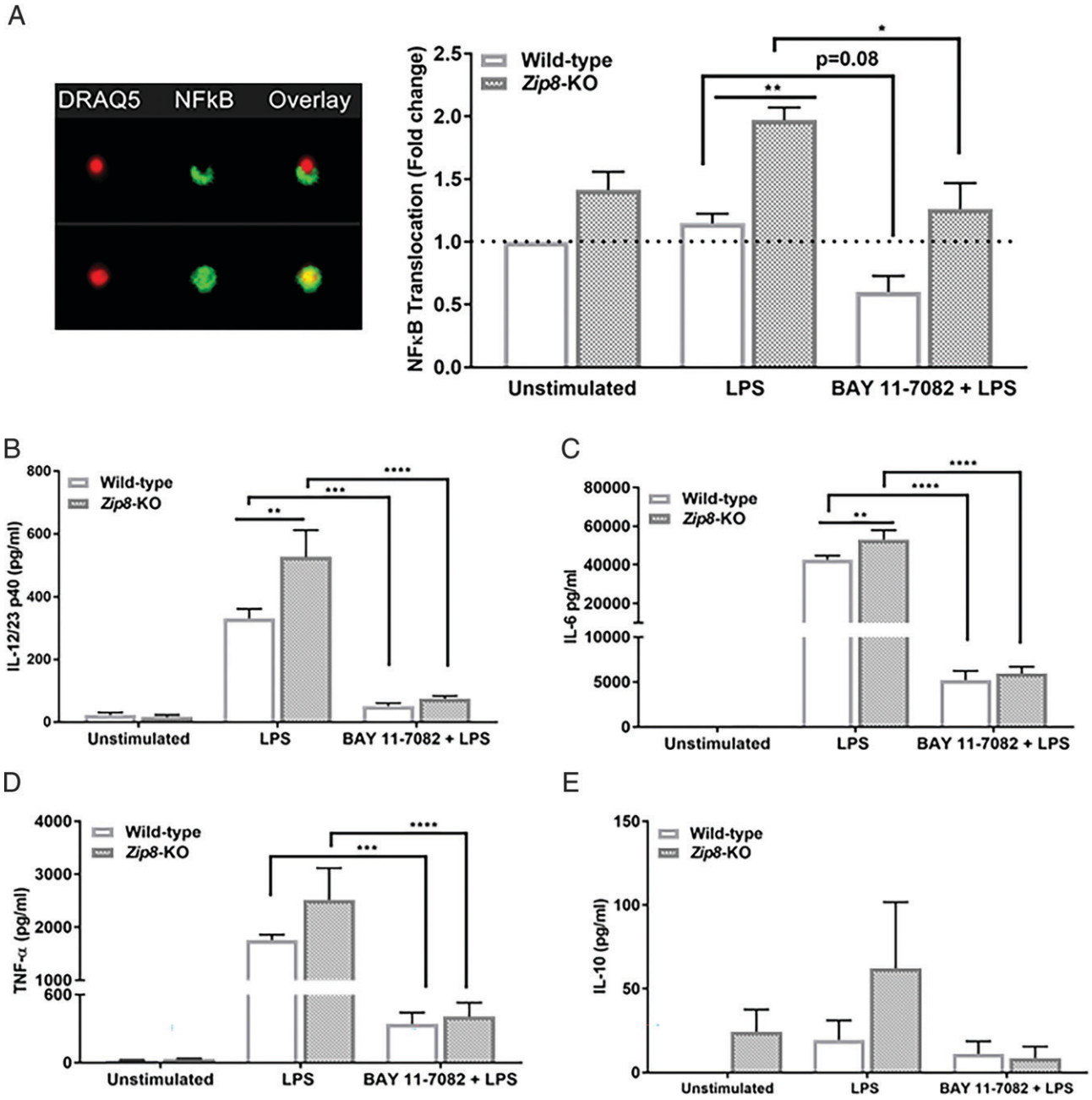

FIGURE 8. NF-κB signaling and corresponding cytokine production are greater in *Zip8*-KO BMDCs after LPS stimulation. BMDCs from WT and *Zip8*-KO animals were stimulated with LPS (1 μg/ml) only or also with an IKK inhibitor (BAY 11-7082; 10 μM) for 1 h, followed by LPS stimulation. At the indicated time points, cells were harvested, fixed, permeabilized, stained, and analyzed by flow cytometry, and supernatants were collected for analysis of cytokine production. (**A**) Fold change in NF-κB nuclear translocation following BAY 11-7082 inhibition for 1 h and/or LPS stimulation (1 μg/ml) for 15 min in WT and *Zip8*-KO BMDCs. NF-κB p65 FITC (green), nuclear dye DRAQ5 (red), and nuclear NF-κB (yellow). (**B–E**) Cytokine profiles from WT and *Zip8*-KO BMDC cultures following ±BAY 11-7082 and then LPS stimulation for 6 h. Data are presented as the mean ± SEM and represent two independent studies. $n = 6–12$ samples per group. $*p \leq 0.05$, $**p < 0.01$, $***p < 0.001$, $****p < 0.0001$.

postinfection and intensified over a period of days. Strikingly, mortality in *Zip8*-KO mice occurred between 72 and 96 h postinfection. During the first 72 h postinfection, an increase in the numbers of AMs and DCs in the lungs of *Zip8*-KO animals occurred. AMs have well-established roles in the host defense against *S. pneumoniae* and subsequent resolution of the inflammatory response (27–30). Interestingly, an increase in numbers of AMs was associated with increased bacterial burdens in the spleens of *Zip8*-KO mice, indicating that *S. pneumoniae* more readily extravasated out of lung into the systemic circulation, resulting in deposition in other tissues. Our previous studies have shown that after bacterial challenge, ZIP8 is significantly upregulated in monocytes and macrophages. This is associated with increased intracellular Zn in these cells, a response that is significantly diminished with small interfering RNA knockdown of ZIP8 (19, 20). Others have shown that the level of intracellular Zn influences the phagocytic capacity of macrophages. In human subjects, Zn deficiency in AMs (caused by alcohol abuse) was shown to impair immune function because of decreased phagocytosis and bacterial clearance (43). More recently, ZIP7 knockdown in THP-1 cells was associated with decreased intracellular Zn and impaired phagocytosis efficiency (44).

Although impaired macrophage phagocytosis is likely a cause of increased bacterial dissemination, aberrant increase in lung DC

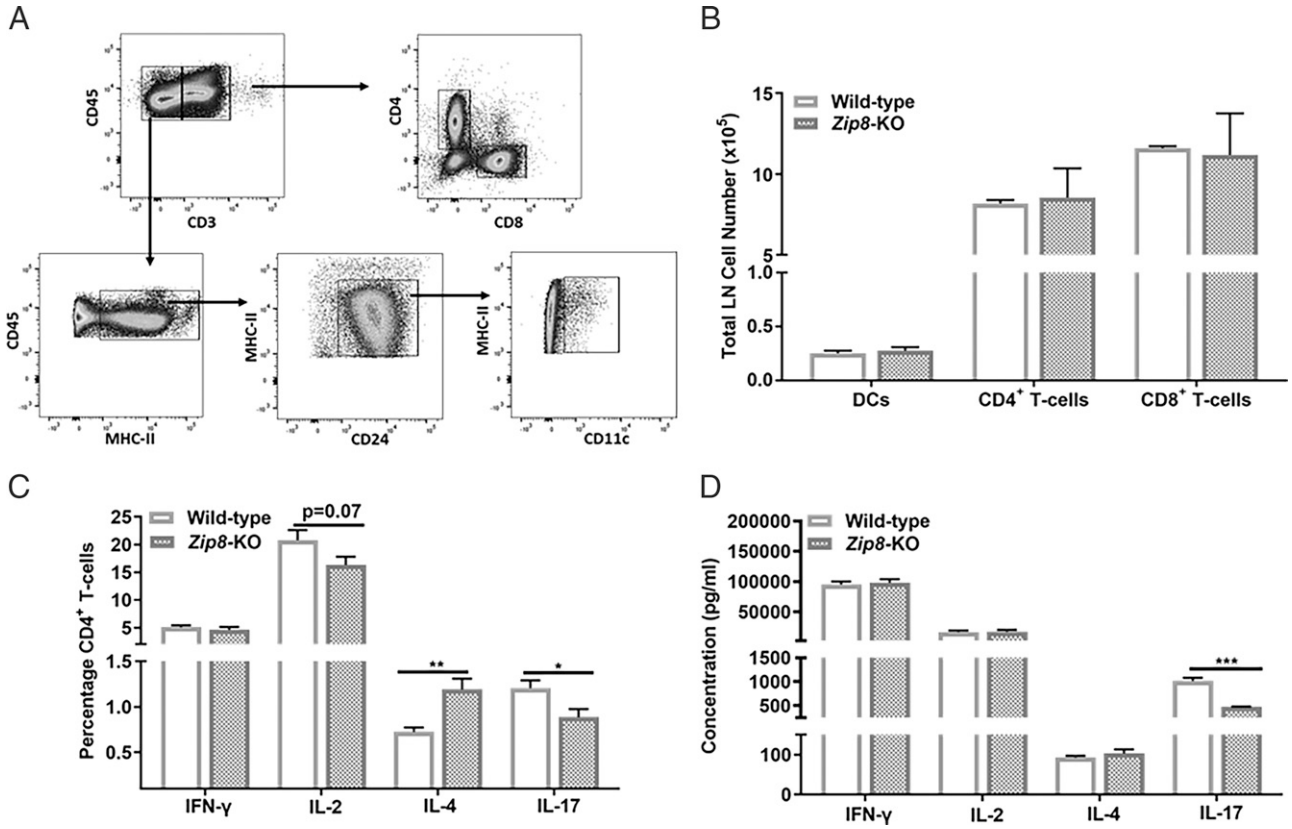

FIGURE 9. Zip8 loss alters communication between DCs and T cells. WT and *Zip8*-KO mice were infected with 4×10^8 CFUs *S. pneumoniae* and mediastinal lymph nodes harvested 72 h postinfection. In some experiments, cells were restimulated in vitro with PMA (10 ng/ml) and ionomycin (250 ng/ml) for the indicated time points with or without brefeldin A (5 μg/ml). (**A**) Gating strategy used to phenotype DCs and T cells and (**B**) quantification of total DCs ($CD8\alpha^+$ and $CD8\alpha^-$ subsets), $CD4^+$ T cells, and $CD8^+$ T cells from LN homogenates of infected mice. (**C**) Th cell cytokine production from $CD4^+$ T cell subsets (with brefeldin A for 4 h) and (**D**) whole LN mixed cell cultures (without brefeldin A for 48 h) from infected WT and *Zip8*-KO animals. Data are presented as the mean ± SEM and represent two independent studies. $n = 14$ animals per group. $^*p < 0.05$, $^{**}p < 0.01$ $^{***}p < 0.001$.

presence has also been shown to exacerbate the immune response and facilitate extrapulmonary dissemination of bacteria during pneumococcal infection (33, 34). Consistent with this, we observed an increase in the $CD11b^+$ subset of lung DCs in *Zip8*-KO mice following *S. pneumoniae* infection. $CD11b^+$ DCs, both conventional and monocyte derived, have been shown to be induced after allergen exposure (45), viral (46), and fungal infection (47) and were found to be the major subset of DCs that transport *Mycobacterium tuberculosis* to the mediastinal lymph following infection (48). Through the process of Ag presentation following infection, DCs have also been shown to act as an "Achilles heel" or "Trojan horse" of the immune system, inadvertently serving as a vehicle for systemic dissemination of pathogens that migrate from the periphery to secondary lymphoid organs (49–52). Whether this response is exacerbated because of ZIP8 loss requires further study.

It is also important to recognize that neutrophils may also contribute to increased bacterial dissemination observed in the *Zip8*-KO animals following pneumococcal infection. Although we did not observe significant differences in polymorphonuclear leukocytes counts between treatment groups, Zn signals have been shown to play an integral role in reactive oxygen species–dependent signal transduction, leading to neutrophil extracellular trap formation and subsequent bacterial killing (53). Therefore, further studies are warranted to determine whether phagocytosis and/or neutrophil extracellular trap formation is impaired because of ZIP8 loss. Nevertheless, the increased presence of macrophages and DCs observed in *Zip8*-KO mice occurred in tandem with more inflammation and cell death. This suggests that worse outcomes following pneumococcal pneumonia in the setting of ZIP8 loss are likely a combination of aberrant immune cell function, mediated in part by these two dominant myeloid cell populations, as well as increased collateral tissue damage caused by an exaggerated immune response.

To our knowledge, we provide novel evidence that ZIP8 is significantly induced in DCs by bacteria, a response unique among other Zn transporters (19, 21). To our knowledge, there has been only one other study that examined the impact of Zn homeostasis on DC function. Kitamura and colleagues (54) revealed that activation of the TLR4 pathway overall decreased DC cytosolic Zn content, which was essential for MHC-II vesicle trafficking and Ag presentation. This phenomenon required downmodulation of ZIP6 expression. Consistent with this, we observed a modest reduction in *Zip6* gene expression in both groups, although not significantly different between the groups. Collectively, the changes in Zn transporter expression resulted in a reduction of available Zn levels, and more so in *Zip8*-KO BMDCs, leading to profound changes in cytokine production in response to bacterial stimulation. These results are in line with previous work in which *Zip8* knockdown resulted in a reduction of cytosolic Zn in macrophages (19). However, in contrast, further modulation of Zn content did not significantly alter cytokine secretion. This suggests that regulation of DC Zn homeostasis is more sophisticated than just a "wholesale" reduction in cellular Zn content. Given that ZIP8 is also a transporter of other divalent ions, including manganese and iron (55–58), it is plausible that some of the ZIP8-mediated changes observed in DCs are not

exclusively attributed to alteration of Zn transport. Further studies are warranted to determine the potential contribution of other divalent metal cations, as well as changes in other Zn transporters, to account for the observed alterations following loss of ZIP8 in DCs.

Notwithstanding, we believe that our data suggest that changes in ZIP8 expression lead to Zn redistribution within macrophages, as previously reported (19), as well as DCs at the onset of infection resulting in modulation of molecular signaling pathways that balance the host immune response. Perhaps most striking, LPS-stimulated *Zip8*-KO DCs exhibited significant alteration in immune-related gene expression profiles that collectively (using IPA) predicted alteration in pathways associated with DC maturation and MHC-II Ag presentation. Notably, the genes with the greatest fold increase in the *Zip8*-KO cells (CD74 and H2-Ab1) play a role in the assembly and transport of the MHC-II molecule. Further studies are warranted to determine whether Ag presentation by MHC-II is altered in *Zip8*-KO DCs because cell surface expression, as characterized by flow cytometry, was similar between the stimulated groups. The predicted alterations in maturation/Ag presentation in *Zip8*-KO DCs were also associated with a concomitant significant increase in NF-κB signaling when compared with WT DCs. NF-κB is induced by many activators of DC maturation and has a well-established role in DC function (42, 59–61). Our group has shown that ZIP8 is a negative and essential regulator of NF-κB signaling and that it tempers activation in a Zn-dependent manner. Studies using monocytes, macrophages, and human lung epithelial cells found that *Zip*8 transcription is directly regulated by NF-κB and suppression of *Zip*8 resulted in increased proinflammatory mediators and increased phosphorylation of p65 and IκBα (20). Consistent with these results, we observed a significant increase in NF-κB nuclear translocation and consequent cytokine production after LPS stimulation, which was significantly ablated by inhibition of NF-κB signaling. These findings are significant in the context of DC function given that NF-κB is required for DC development, survival, activation, and T cell priming (42, 61, 62). Previous studies have shown that MAPKs, specifically p38 and ERK1/2, play a role in DC cytokine production after bacterial stimulation; however, the extent of ERK and p38 phosphorylation was no different between stimulated WT and *Zip8*-KO BMDC cultures. Taken together, this demonstrates that ZIP8 loss in DCs results in increased NF-κB activation, similar to what is seen in macrophages, which is a major contributor to aberrant immune function.

Given the vital role that DCs play in bacterial recognition and initiation of the adaptive immune response, we wanted to begin to understand whether ZIP8, or lack thereof, may have a broader impact beyond frontline host defense. In accordance with this, we observed that $CD4^+$ T cells from the lymph nodes of *Zip8*-KO–infected animals were impaired in their ability to produce IL-17. Over the last two decades, a protective role of IL-17–producing $CD4^+$ Th17 cells in the host immune response against pneumococcal infection has emerged. It has been shown that local production of IL-17 plays a significant role in mounting an effective host defense against bacteria by promoting neutrophil and macrophage recruitment, thus enhancing pneumococcal clearance by phagocytes (63, 64). IL-17A has also been shown to stimulate epithelial cells to trigger antimicrobial responses against intracellular bacteria, and increased mortality was observed in mice with a deficiency in the IL-17RA postinfection with *S. pneumoniae* TIGR-4 strain (65). Decreased levels of IL-17A were also found to be associated with increased risk of bacteremia in a *Klebsiella pneumoniae* model (66). In the context of our findings, increased IL-4 production from $CD4^+$ T cells isolated from the LNs of *Zip8*-KO mice may also contribute further to inhibition of a protective Th17/IL-17 response, which we believe is detrimental to the host. Consistent with this, increased production of IL-4 is associated with systemic bacterial infection and increased mortality following pneumococcal infection (67, 68), with increased bacterial clearance and survival in IL-4–deficient mice following bacterial pneumonia (69). We postulate that the diminished IL-17 response has broader implications in the context of memory responses and long-term protection against pneumococcal infections. Consistent with this, a recent study demonstrated that protection against different *S. pneumoniae* serotypes was mediated primarily by Th17 cells and not Abs. Immune mice were shown to mount an even stronger IL-17A response compared with initial infection. In addition, the localized Th cell lung response consisted mainly of IL-17A–producing $CD4^+$ T cells, with only a small proportion of IFN-γ–producing $CD4^+$ T cells (70).

Although macrophages are recognized as APCs, DCs are considered more so as professional APCs that capture Ags in the periphery, migrate to the draining LNs, and then present Ags to naive T cells, thus bridging the gap between innate and adaptive immunity. Based on our findings, we contend that T cell priming in the lung draining mediastinal lymph nodes of *S. pneumoniae*–infected mice is mediated primarily by DCs and that loss of ZIP8 contributes to an impaired Th cell response. Given that appropriate T cell priming is fundamental to activation of the adaptive immune response, future studies are warranted to further elucidate the mechanisms by which ZIP8 mediates T cell priming/activation, specifically Th17 activation, in the host response against pneumococcal pneumonia. Notwithstanding, these results highlight a complex and vital role for ZIP8-mediated Zn homeostasis relative to cell-to-cell communication.

Zn is required for proper immune function, and dietary-induced deficiency is associated with increased susceptibility to pneumococcal infection (12, 13). For example, to combat invading pathogens, the host upregulates the acquisition of critical nutrients (Zn, iron, etc.), a defense known as "nutritional immunity." Whereas this is classically associated with the restriction of iron, the availability of other transition metals, including manganese and Zn, are also highly regulated by the host. To acquire sufficient Zn, most bacteria possess homologs of Znu/Adc, an ATP-binding cassette (ABC) permease system capable of directly importing labile Zn with nanomolar affinity. These systems are important for the virulence of numerous pathogens, including *S. pneumoniae* (71–73). We postulate that ZIP8 is upregulated at the onset of bacterial infection, resulting in redistribution of Zn within host immune cells. This provides a competitive advantage to the host through immune cell recruitment to contain infection. In the absence of ZIP8 and therefore Zn, this response is substantially augmented, ultimately resulting in acute and possibly long-term outcomes following pneumococcal pneumonia. This is supported by a recent GWAS in humans that identified a polymorphic variant of *Zip*8 was significantly associated with increased susceptibility to *S. aureus* infection (24). This is further supported by a recent study in which dietary Zn deficiency enhanced susceptibility to pneumococcal infection in mice caused by alteration of phagocytic function resulting in bacterial dissemination (74). A common genetic variant in ZIP8 (rs13107325; A391T) ranks in the top 10 of pleiotropic single nucleotide polymorphisms identified in GWAS, and in silico modeling predicts rs13107325 to be in the top 1.4% of deleterious substitutions in the human genome (75). Given the relatively high frequency of its occurrence and recent studies demonstrating that this ZIP8 variant is commonly associated as a driver of inflammation-based disease (76), we believe our findings to be clinically relevant. Also, given the relatively high occurrence of dietary Zn deficiency in populations that are most susceptible to pneumococcal pneumonia, further studies are warranted to determine whether patients that harbor the A391T allele and who have poor dietary Zn intake are even more prone to infection and worse

outcomes and whether either or both can be countered with aggressive Zn supplementation strategies.

Taken together, this investigation highlights a previously unidentified link between Zn homoeostasis, myeloid immune cell function, and the host response against pneumococcus in the lung. Our (to our knowledge) novel findings, substantiate that a decrease in available Zn is required for proper DC function but that there also exists an essential ZIP8-dependent, Zn-mediated balance between cellular activation machinery and adaptive immune priming. This further underscores the complexity of essential divalent metal trafficking, not limited to Zn, as a vital component of immune regulation in the battle between host and pathogen. It also warrants future studies that evaluate the impact of both environment (dietary nutrient intake) and genetic composition (for example, Zn regulatory factors) in tandem in the context of host susceptibility to and recovery from infection with commonly occurring pathogens.

Acknowledgments

We thank members of the Tissue Sciences Facility at the Department of Pathology and Microbiology Department (UNMC) for assistance with lung tissue processing, sectioning, and H&E staining and assistance with digital microscopy images prepared for the manuscript.

Disclosures

The authors have no financial conflicts of interest.

References

1. File, T. M., Jr., D. E. Low, P. B. Eckburg, G. H. Talbot, H. D. Friedland, J. Lee, L. Llorens, I. Critchley, and D. Thye. 2010. Integrated analysis of FOCUS 1 and FOCUS 2: randomized, doubled-blinded, multicenter phase 3 trials of the efficacy and safety of ceftaroline fosamil versus ceftriaxone in patients with community-acquired pneumonia. *Clin. Infect. Dis.* 51: 1395–1405.
2. Musher, D. M., I. L. Roig, G. Cazares, C. E. Stager, N. Logan, and H. Safar. 2013. Can an etiologic agent be identified in adults who are hospitalized for community-acquired pneumonia: results of a one-year study. *J. Infect.* 67: 11–18.
3. Restrepo, M. I., E. M. Mortensen, J. A. Velez, C. Frei, and A. Anzueto. 2008. A comparative study of community-acquired pneumonia patients admitted to the ward and the ICU. *Chest* 133: 610–617.
4. Sherwin, R. L., S. Gray, R. Alexander, P. C. McGovern, J. Graepel, M. W. Pride, J. Purdy, P. Paradiso, and T. M. File, Jr. 2013. Distribution of 13-valent pneumococcal conjugate vaccine *Streptococcus pneumoniae* serotypes in US adults aged ≥50 years with community-acquired pneumonia. *J. Infect. Dis.* 208: 1813–1820.
5. Gonçalves, M. T., T. J. Mitchell, and J. M. Lord. 2016. Immune ageing and susceptibility to *Streptococcus pneumoniae*. *Biogerontology* 17: 449–465.
6. Rink, L., and H. Kirchner. 2000. Zinc-altered immune function and cytokine production. *J. Nutr.* 130(5S, Suppl)1407S–1411S.
7. Ibs, K. H., and L. Rink. 2003. Zinc-altered immune function. *J. Nutr.* 133(5, Suppl 1)1452S–1456S.
8. Fraker, P. J., L. E. King, T. Laakko, and T. L. Vollmer. 2000. The dynamic link between the integrity of the immune system and zinc status. *J. Nutr.* 130(5S Suppl)1399S–1406S.
9. Fraker, P. J., and L. E. King. 2004. Reprogramming of the immune system during zinc deficiency. *Annu. Rev. Nutr.* 24: 277–298.
10. Wessells, K. R., and K. H. Brown. 2012. Estimating the global prevalence of zinc deficiency: results based on zinc availability in national food supplies and the prevalence of stunting. *PLoS One* 7: e50568.
11. Fischer Walker, C., and R. E. Black. 2004. Zinc and the risk for infectious disease. *Annu. Rev. Nutr.* 24: 255–275.
12. Mocchegiani, E., R. Giacconi, M. Muzzioli, and C. Cipriano. 2000. Zinc, infections and immunosenescence. *Mech. Ageing Dev.* 121: 21–35.
13. Barnett, J. B., D. H. Hamer, and S. N. Meydani. 2010. Low zinc status: a new risk factor for pneumonia in the elderly? *Nutr. Rev.* 68: 30–37.
14. Girodon, F., P. Galan, A. L. Monget, M. C. Boutron-Ruault, P. Brunet-Lecomte, P. Preziosi, J. Arnaud, J. C. Manuguerra, and S. Herchberg. 1999. Impact of trace elements and vitamin supplementation on immunity and infections in institutionalized elderly patients: a randomized controlled trial. MIN. VIT. AOX. geriatric network. *Arch. Intern. Med.* 159: 748–754.
15. Girodon, F., M. Lombard, P. Galan, P. Brunet-Lecomte, A. L. Monget, J. Arnaud, P. Preziosi, and S. Hercberg. 1997. Effect of micronutrient supplementation on infection in institutionalized elderly subjects: a controlled trial. *Ann. Nutr. Metab.* 41: 98–107.
16. Prasad, A. S., F. W. Beck, B. Bao, J. T. Fitzgerald, D. C. Snell, J. D. Steinberg, and L. J. Cardozo. 2007. Zinc supplementation decreases incidence of infections in the elderly: effect of zinc on generation of cytokines and oxidative stress. *Am. J. Clin. Nutr.* 85: 837–844.
17. Bafaro, E., Y. Liu, Y. Xu, and R. E. Dempski. 2017. The emerging role of zinc transporters in cellular homeostasis and cancer. *Signal Transduct. Target. Ther.* 2: 17029.
18. Hojyo, S., and T. Fukada. 2016. Zinc transporters and signaling in physiology and pathogenesis. *Arch. Biochem. Biophys.* 611: 43–50.
19. Pyle, C. J., S. Akhter, S. Bao, C. E. Dodd, L. S. Schlesinger, and D. L. Knoell. 2017. Zinc modulates endotoxin-induced human macrophage inflammation through ZIP8 induction and C/EBPβ inhibition. *PLoS One* 12: e0169531.
20. Liu, M. J., S. Bao, M. Gálvez-Peralta, C. J. Pyle, A. C. Rudawsky, R. E. Pavlovicz, D. W. Killilea, C. Li, D. W. Nebert, M. D. Wewers, and D. L. Knoell. 2013. ZIP8 regulates host defense through zinc-mediated inhibition of NF-κB. *Cell Rep.* 3: 386–400.
21. Pyle, C. J., A. K. Azad, A. C. Papp, W. Sadee, D. L. Knoell, and L. S. Schlesinger. 2017. Elemental ingredients in the macrophage cocktail: role of ZIP8 in host response to *Mycobacterium tuberculosis*. *Int. J. Mol. Sci.* 18: 2375.
22. Costas, J. 2018. The highly pleiotropic gene SLC39A8 as an opportunity to gain insight into the molecular pathogenesis of schizophrenia. *Am. J. Med. Genet. B. Neuropsychiatr. Genet.* 177: 274–283.
23. Pickrell, J. K., T. Berisa, J. Z. Liu, L. Ségurel, J. Y. Tung, and D. A. Hinds. 2016. Detection and interpretation of shared genetic influences on 42 human traits. [Published erratum appears in 2016 *Nat. Genet.* 48: 1296.] *Nat. Genet.* 48: 709–717.
24. Ye, Z., D. A. Vasco, T. C. Carter, M. H. Brilliant, S. J. Schrodi, and S. K. Shukla. 2014. Genome wide association study of SNP-, gene-, and pathway-based approaches to identify genes influencing susceptibility to *Staphylococcus aureus* infections. *Front. Genet.* 5: 125.
25. Guilliams, M., B. N. Lambrecht, and H. Hammad. 2013. Division of labor between lung dendritic cells and macrophages in the defense against pulmonary infections. *Mucosal Immunol.* 6: 464–473.
26. Kopf, M., C. Schneider, and S. P. Nobs. 2015. The development and function of lung-resident macrophages and dendritic cells. *Nat. Immunol.* 16: 36–44.
27. Aberdein, J. D., J. Cole, M. A. Bewley, H. M. Marriott, and D. H. Dockrell. 2013. Alveolar macrophages in pulmonary host defence the unrecognized role of apoptosis as a mechanism of intracellular bacterial killing. *Clin. Exp. Immunol.* 174: 193–202.
28. Dockrell, D. H., H. M. Marriott, L. R. Prince, V. C. Ridger, P. G. Ince, P. G. Hellewell, and M. K. Whyte. 2003. Alveolar macrophage apoptosis contributes to pneumococcal clearance in a resolving model of pulmonary infection. *J. Immunol.* 171: 5380–5388.
29. Guillon, A., E. I. Arafa, K. A. Barker, A. C. Belkina, I. Martin, A. T. Shenoy, A. K. Wooten, C. Lyon De Ana, A. Dai, A. Labadorf, et al. 2020. Pneumonia recovery reprograms the alveolar macrophage pool. *JCI Insight* 5: e133042.
30. Knapp, S., J. C. Leemans, S. Florquin, J. Branger, N. A. Maris, J. Pater, N. van Rooijen, and T. van der Poll. 2003. Alveolar macrophages have a protective anti-inflammatory role during murine pneumococcal pneumonia. *Am. J. Respir. Crit. Care Med.* 167: 171–179.
31. Hammad, H., and B. N. Lambrecht. 2007. Lung dendritic cell migration. *Adv. Immunol.* 93: 265–278.
32. Worbs, T., S. I. Hammerschmidt, and R. Förster. 2017. Dendritic cell migration in health and disease. *Nat. Rev. Immunol.* 17: 30–48.
33. Winter, C., K. Taut, F. Länger, M. Mack, D. E. Briles, J. C. Paton, R. Maus, M. Srivastava, T. Welte, and U. A. Maus. 2007. FMS-like tyrosine kinase 3 ligand aggravates the lung inflammatory response to *Streptococcus pneumoniae* infection in mice: role of dendritic cells. *J. Immunol.* 179: 3099–3108.
34. Rosendahl, A., S. Bergmann, S. Hammerschmidt, O. Goldmann, and E. Medina. 2013. Lung dendritic cells facilitate extrapulmonary bacterial dissemination during pneumococcal pneumonia. *Front. Cell. Infect. Microbiol.* 3: 21.
35. Knoell, D. L., D. Smith, S. Bao, M. Sapkota, T. A. Wyatt, J. L. Zweier, J. Flury, M. T. Borchers, and M. Knutson. 2020. Imbalance in zinc homeostasis enhances lung tissue loss following cigarette smoke exposure. *J. Trace Elem. Med. Biol.* 60: 126483.
36. Trouplin, V., N. Boucherit, L. Gorvel, F. Conti, G. Mottola, and E. Ghigo. 2013. Bone marrow-derived macrophage production. *J. Vis. Exp.* 81: e50966.
37. Inaba, K., M. Inaba, N. Romani, H. Aya, M. Deguchi, S. Ikehara, S. Muramatsu, and R. M. Steinman. 1992. Generation of large numbers of dendritic cells from mouse bone marrow cultures supplemented with granulocyte/macrophage colony-stimulating factor. *J. Exp. Med.* 176: 1693–1702.
38. Livak, K. J., and T. D. Schmittgen. 2001. Analysis of relative gene expression data using real-time quantitative PCR and the 2(-delta delta C(T)) method. *Methods* 25: 402–408.
39. Dyavar, S. R., T. M. Mykris, L. C. Winchester, K. K. Scarsi, C. V. Fletcher, and A. T. Podany. 2020. Hepatocytic transcriptional signatures predict comparative drug interaction potential of rifamycin antibiotics. *Sci. Rep.* 10: 12565.
40. Dyavar, S. R., L. F. Potts, G. Beck, B. L. Dyavar Shetty, B. Lawson, A. T. Podany, C. V. Fletcher, R. R. Amara, and S. M. Papa. 2020. Transcriptomic approach predicts a major role for transforming growth factor beta type 1 pathway in L-Dopa-induced dyskinesia in parkinsonian rats. *Genes Brain Behav.* 19: e12690.
41. Dyavar Shetty, R., V. Velu, K. Titanji, S. E. Bosinger, G. J. Freeman, G. Silvestri, and R. R. Amara. 2012. PD-1 blockade during chronic SIV infection reduces hyperimmune activation and microbial translocation in rhesus macaques. *J. Clin. Invest.* 122: 1712–1716.
42. O'Sullivan, B. J., and R. Thomas. 2002. CD40 ligation conditions dendritic cell antigen-presenting function through sustained activation of NF-kappaB. *J. Immunol.* 168: 5491–5498.

43. Mehta, A. J., S. M. Yeligar, L. Elon, L. A. Brown, and D. M. Guidot. 2013. Alcoholism causes alveolar macrophage zinc deficiency and immune dysfunction. *Am. J. Respir. Crit. Care Med.* 188: 716–723.
44. Xie, W., Q. Xue, L. Niu, and K. W. Wong. 2020. Zinc transporter SLC39A7 relieves zinc deficiency to suppress alternative macrophage activation and impairment of phagocytosis. *PLoS One* 15: e0235776.
45. Plantinga, M., M. Guilliams, M. Vanheerswynghels, K. Deswarte, F. Branco-Madeira, W. Toussaint, L. Vanhoutte, K. Neyt, N. Killeen, B. Malissen, et al. 2013. Conventional and monocyte-derived CD11b(+) dendritic cells initiate and maintain T helper 2 cell-mediated immunity to house dust mite allergen. *Immunity* 38: 322–335.
46. Lukens, M. V., D. Kruijsen, F. E. Coenjaerts, J. L. Kimpen, and G. M. van Bleek. 2009. Respiratory syncytial virus-induced activation and migration of respiratory dendritic cells and subsequent antigen presentation in the lung-draining lymph node. *J. Virol.* 83: 7235–7243.
47. Osterholzer, J. J., G. H. Chen, M. A. Olszewski, J. L. Curtis, G. B. Huffnagle, and G. B. Toews. 2009. Accumulation of CD11b+ lung dendritic cells in response to fungal infection results from the CCR2-mediated recruitment and differentiation of Ly-6Chigh monocytes. *J. Immunol.* 183: 8044–8053.
48. Wolf, A. J., B. Linas, G. J. Trevejo-Nuñez, E. Kincaid, T. Tamura, K. Takatsu, and J. D. Ernst. 2007. *Mycobacterium tuberculosis* infects dendritic cells with high frequency and impairs their function in vivo. *J. Immunol.* 179: 2509–2519.
49. Bierly, A. L., W. J. Shufesky, W. Sukhumavasi, A. E. Morelli, and E. Y. Denkers. 2008. Dendritic cells expressing plasmacytoid marker PDCA-1 are Trojan horses during *Toxoplasma gondii* infection. *J. Immunol.* 181: 8485–8491.
50. Izquierdo-Useros, N., M. Naranjo-Gómez, I. Erkizia, M. C. Puertas, F. E. Borràs, J. Blanco, and J. Martinez-Picado. 2010. HIV and mature dendritic cells: Trojan exosomes riding the Trojan horse? *PLoS Pathog.* 6: e1000740.
51. Schönrich, G., and M. J. Raftery. 2015. Dendritic cells as Achilles' heel and Trojan horse during varicella zoster virus infection. *Front. Microbiol.* 6: 417.
52. Williams, N. L., J. L. Morris, C. M. Rush, and N. Ketheesan. 2014. Migration of dendritic cells facilitates systemic dissemination of Burkholderia pseudomallei. *Infect. Immun.* 82: 4233–4240.
53. Hasan, R., L. Rink, and H. Haase. 2013. Zinc signals in neutrophil granulocytes are required for the formation of neutrophil extracellular traps. *Innate Immun.* 19: 253–264.
54. Kitamura, H., H. Morikawa, H. Kamon, M. Iguchi, S. Hojyo, T. Fukada, S. Yamashita, T. Kaisho, S. Akira, M. Murakami, and T. Hirano. 2006. Toll-like receptor-mediated regulation of zinc homeostasis influences dendritic cell function. *Nat. Immunol.* 7: 971–977.
55. Choi, E. K., T. T. Nguyen, N. Gupta, S. Iwase, and Y. A. Seo. 2018. Functional analysis of SLC39A8 mutations and their implications for manganese deficiency and mitochondrial disorders. *Sci. Rep.* 8: 3163.
56. Scheiber, I. F., N. O. Alarcon, and N. Zhao. 2019. Manganese uptake by A549 cells is mediated by both ZIP8 and ZIP14. *Nutrients* 11: 1473.
57. van Raaij, S. E. G., S. K. S. Srai, D. W. Swinkels, and R. P. L. van Swelm. 2019. Iron uptake by ZIP8 and ZIP14 in human proximal tubular epithelial cells. *Biometals* 32: 211–226.
58. Wang, C. Y., S. Jenkitkasemwong, S. Duarte, B. K. Sparkman, A. Shawki, B. Mackenzie, and M. D. Knutson. 2012. ZIP8 is an iron and zinc transporter whose cell-surface expression is up-regulated by cellular iron loading. *J. Biol. Chem.* 287: 34032–34043.
59. Dev, A., S. Iyer, B. Razani, and G. Cheng. 2011. NF-κB and innate immunity. *Curr. Top. Microbiol. Immunol.* 349: 115–143.
60. Rescigno, M., M. Martino, C. L. Sutherland, M. R. Gold, and P. Ricciardi-Castagnoli. 1998. Dendritic cell survival and maturation are regulated by different signaling pathways. *J. Exp. Med.* 188: 2175–2180.
61. Ouaaz, F., J. Arron, Y. Zheng, Y. Choi, and A. A. Beg. 2002. Dendritic cell development and survival require distinct NF-kappaB subunits. *Immunity* 16: 257–270.
62. van de Laar, L., A. van den Bosch, S. W. van der Kooij, H. L. Janssen, P. J. Coffer, C. van Kooten, and A. M. Woltman. 2010. A nonredundant role for canonical NF-κB in human myeloid dendritic cell development and function. *J. Immunol.* 185: 7252–7261.
63. Marqués, J. M., A. Rial, N. Muñoz, F. X. Pellay, L. Van Maele, H. Léger, T. Camou, J. C. Sirard, A. Benecke, and J. A. Chabalgoity. 2012. Protection against *Streptococcus pneumoniae* serotype 1 acute infection shows a signature of Th17- and IFN-γ-mediated immunity. *Immunobiology* 217: 420–429.
64. Wang, W., A. Zhou, X. Zhang, Y. Xiang, Y. Huang, L. Wang, S. Zhang, Y. Liu, Y. Yin, and Y. He. 2014. Interleukin 17A promotes pneumococcal clearance by recruiting neutrophils and inducing apoptosis through a p38 mitogen-activated protein kinase-dependent mechanism in acute otitis media. *Infect. Immun.* 82: 2368–2377.
65. Ritchie, N. D., R. Ritchie, H. K. Bayes, T. J. Mitchell, and T. J. Evans. 2018. IL-17 can be protective or deleterious in murine pneumococcal pneumonia. *PLoS Pathog.* 14: e1007099.
66. Ye, P., P. B. Garvey, P. Zhang, S. Nelson, G. Bagby, W. R. Summer, P. Schwarzenberger, J. E. Shellito, and J. K. Kolls. 2001. Interleukin-17 and lung host defense against *Klebsiella pneumoniae* infection. *Am. J. Respir. Cell Mol. Biol.* 25: 335–340.
67. Mizrachi-Nebenzahl, Y., S. Lifshitz, R. Teitelbaum, S. Novick, A. Levi, D. Benharroch, E. Ling, and R. Dagan. 2003. Differential activation of the immune system by virulent *Streptococcus pneumoniae* strains determines recovery or death of the host. *Clin. Exp. Immunol.* 134: 23–31.
68. Woytschak, J., N. Keller, C. Krieg, D. Impellizzieri, R. W. Thompson, T. A. Wynn, A. S. Zinkernagel, and O. Boyman. 2016. Type 2 interleukin-4 receptor signaling in neutrophils antagonizes their expansion and migration during infection and inflammation. *Immunity* 45: 172–184.
69. Song, Z., J. Zhang, X. Zhang, D. Li, H. Wang, X. Xu, W. Xu, Y. Yin, and J. Cao. 2015. Interleukin 4 deficiency reverses development of secondary *Pseudomonas aeruginosa* pneumonia during sepsis-associated immunosuppression. *J. Infect. Dis.* 211: 1616–1627.
70. Wang, Y., B. Jiang, Y. Guo, W. Li, Y. Tian, G. F. Sonnenberg, J. N. Weiser, X. Ni, and H. Shen. 2017. Cross-protective mucosal immunity mediated by memory Th17 cells against *Streptococcus pneumoniae* lung infection. *Mucosal Immunol.* 10: 250–259.
71. Bayle, L., S. Chimalapati, G. Schoehn, J. Brown, T. Vernet, and C. Durmort. 2011. Zinc uptake by *Streptococcus pneumoniae* depends on both AdcA and AdcAII and is essential for normal bacterial morphology and virulence. *Mol. Microbiol.* 82: 904–916.
72. Brown, L. R., R. C. Caulkins, T. E. Schartel, J. W. Rosch, E. S. Honsa, S. Schultz-Cherry, V. A. Meliopoulos, S. Cherry, and J. A. Thornton. 2017. Increased zinc availability enhances initial aggregation and biofilm formation of *Streptococcus pneumoniae*. *Front. Cell. Infect. Microbiol.* 7: 233.
73. Makthal, N., H. Do, B. M. Wendel, R. J. Olsen, J. D. Helmann, J. M. Musser, and M. Kumaraswami. 2020. Group A Streptococcus AdcR regulon participates in bacterial defense against host-mediated zinc sequestration and contributes to virulence. *Infect. Immun.* 88: e00097-20. doi: 10.1128/IAI.00097-20. Print 2020 Jul 21.
74. Eijkelkamp, B. A., J. R. Morey, S. L. Neville, A. Tan, V. G. Pederick, N. Cole, P. P. Singh, C. Y. Ong, R. Gonzalez de Vega, D. Clases, et al. 2019. Dietary zinc and the control of *Streptococcus pneumoniae* infection. *PLoS Pathog.* 15: e1007957.
75. Zhang, R., K. Witkowska, J. Afonso Guerra-Assunção, M. Ren, F. L. Ng, C. Mauro, A. T. Tucker, M. J. Caulfield, and S. Ye. 2016. A blood pressure-associated variant of the SLC39A8 gene influences cellular cadmium accumulation and toxicity. *Hum. Mol. Genet.* 25: 4117–4126.
76. Sunuwar, L., A. Frkatović, S. Sharapov, Q. Wang, H. M. Neu, X. Wu, T. Haritunians, F. Wan, S. Michel, S. Wu, et al. 2020. Pleiotropic ZIP8 A391T implicates abnormal manganese homeostasis in complex human disease. *JCI Insight* 5: e140978.